Performance Analysis of OFDM and OTFS Waveforms in Doubly-Spread Channels

Niladri Halder, *Graduate Student Member, IEEE* and Chandra R. Murthy, *Fellow, IEEE*

***Abstract*—Orthogonal frequency division multiplexing (OFDM) and orthogonal time frequency space (OTFS) are among the most intensively researched communication waveforms in the literature, yet comprehensive studies of how the waveforms determine their relative performance under different channel conditions remain limited. In this paper, we introduce the notions of symbol spreading (SS) and interference spreading (IS) to develop a time-frequency (TF)-domain analytical model for both OFDM and OTFS. We derive explicit expressions for the SS and IS and elucidate their behavior across different channel conditions with varying delay and Doppler spreads. It reveals the distinct SS-IS characteristics of OFDM and OTFS, and their effects on the TF diversity, signal-to-interference ratio, and BER. We then analyze how SS and IS affect data detection with interference-agnostic and interference-suppressing equalizers, and in both uncoded and coded transmissions. In coded communication, to enable reliable soft-symbol decoding, we propose a novel low-complexity variational Bayesian log-likelihood ratio (VB-LLR) detector and study the impact of soft-symbol quality at different code rates. Our theoretical analysis and simulations reveal interesting insights on (a) the relative performance of OFDM and OTFS over a wide range of delay and Doppler spreads; (b) the superiority of OTFS in uncoded communication; and (c) how channel coding enables OFDM to achieve performance comparable to OTFS at moderate code rates and even outperform OTFS at lower code rates, with the VB-LLR detector.**

***Index Terms*—symbol-spreading, interference spreading, time frequency diversity, delay effect, Doppler effect.**

I. Introduction

ORthogonal frequency division multiplexing (OFDM) has been the waveform of choice in 4G and 5G cellular wireless systems (and 6G also) due to its low-complexity receiver architecture and efficient practical implementation [1]. However, OFDM diagonalizes the channel–and hence enables low-complexity equalization–only in purely delay-spread scenarios with negligible Doppler spread. However, next-generation wireless systems target high-mobility communication scenarios [2], [3] where the multipath Doppler shifts lead to delay-Doppler (DD)-spread channels. Under such conditions, OFDM loses its diagonal structure due to severe inter-carrier interference (ICI), causing significant performance degradation [4].

Orthogonal time-frequency space (OTFS) modulation [5], [6] has been recently proposed as an alternative waveform, and has been shown to outperform OFDM in DD-spread channels. However, unlike OFDM in purely delay-spread channels, OTFS does not diagonalize DD-spread channels and hence requires sophisticated equalization techniques to obtain the performance benefits. This raises a fundamental question: *is there an intrinsic mechanism that enables OTFS to outperform OFDM, or does the superiority of OTFS stem from the more sophisticated equalizer employed?* To address this, we introduce the notions of *symbol spreading (SS)*, quantifying how the modulation scheme intends to spread a transmitted symbol over the time–frequency (TF) domain after propagation through a DD-spread channel, and *interference spreading (IS)*, which characterizes the unintended residual spreading of the symbol over the TF domain, resulting in interference to all other symbols. Using this, we analyze the relative performance of OFDM and OTFS across different channel conditions and equalizers, and elucidate the fundamental reasons behind their observed performance trends in both uncoded and coded transmissions.

A. Related Work and Motivation

1) Uncoded Communications: In [4], [6], [7], uncoded OFDM and OTFS are empirically compared over DD-spread channels; however, the underlying reasons for their relative performance are not analyzed. The DD-domain diversity of OTFS is investigated in [8], [9], motivating the notion of SS, but the impact of interference power on performance is not examined. In contrast, [7], [10] focus on the computation of ICI and inter-symbol interference (ISI) powers in OTFS. Further, [11] shows that OTFS performance depends not only on the interference power but also on the number of interfering symbols in the DD domain, motivating the notion of IS; however, its impact on performance under different equalizers is not analyzed. The joint influence and trade-offs of SS-induced diversity, interference power, and IS on waveform performance across equalizer architectures remain unexplored.

Advanced OTFS receiver designs for mitigating DD-domain interference are developed in [12]–[14], without direct performance comparisons with OFDM under the same equalization frameworks. Comparisons under similar complexity equalizers are presented in [15], [16]. While [15] considers a message passing (MP) equalizer and observes a pronounced performance gap between OTFS and OFDM, [16] shows that low complexity 1-tap equalization leads to BER floors for both waveforms. The dependence of the relative performance gap on receiver complexity, therefore, remains unundersto od. The impact of mobility on OTFS performance is examined in [7] through simulations at a few maximum velocities, while [17] considers variations in delay spread $\tau_{\max}$ and Doppler spread $\nu_{\max}$ over a limited range and reports robustness of OTFS

The authors are with the Department of Electrical Communication Engineering, Indian Institute of Science, Bengaluru 560012, India (e-mails: niladrih@iisc.ac.in; cmurthy@iisc.ac.in).

TABLE I: Summary of literature on the analysis of OFDM and OTFS performance in uncoded and coded communications.

	[4], [6], [20]	[7]	[8], [17]	[10]	[11]	[15], [18]	[19], [23]	[9], [21]	[22]	This work
Uncoded comparison	✓	✓	✓	✓	✓	✓	✗	✓	✗	✓
SS-induced diversity	✗	✗	✓	✗	✗	✗	✗	✓	✗	✓
Interference power computation	✗	✓	✗	✓	✓	✗	✗	✗	✓	✓
IS analysis	✗	✗	✗	✗	✓	✗	✗	✗	✗	✓
Coded comparsion	✓	✗	✗	✓	✗	✗	✓	✓	✓	✓
SS-IS on equalizer performance	✗	✗	✗	✗	✗	✗	✗	✗	✗	✓
Soft symbol quality vs. code rate	✗	✗	✗	✗	✗	✗	✗	✗	✗	✓
All channel conditions*	✗	✗	✗	✗	✗	✗	✗	✗	✗	✓

* Flat-fading, purely delay-spread, purely Doppler-spread, and DD-spread channels, including variations in delay and Doppler spreads.

to these parameters. However, it remains unclear whether this robustness extends across a wide range of $\tau_{\max}$ and $\nu_{\max}$, or whether it breaks down in certain operating regimes, as their effects on diversity and interference spreading are not characterized. In addition, [18] shows improved BER of OTFS over OFDM in purely delay-spread channels via simulations, but no theoretical justification is provided. The performance of OFDM and OTFS across different channels has not been analyzed within a unified theoretical framework that also accounts for equalizer complexity. Furthermore, the existence of performance crossover across different channel conditions under different equalizer architectures remains unexplored.

2) Coded Communications: In [4], [19], [20], coded performance comparisons between OFDM and OTFS are presented, without theoretical analysis explaining the observed performance trends. Furthermore, [9], [21] analyze the relative performance of OFDM and OTFS in terms of coding gain and diversity gain, while [10] focuses on ICI power and the resulting signal-to-interference-plus-noise ratio (SINR). Nevertheless, a joint analysis that accounts for symbol diversity, interference power, and their spreading characteristics in coded communications is unavailable. In addition, [22] considers performance through simulations under specific channel conditions at a fixed code rate, while [4], [21], [23] examine a limited set of maximum velocities also at a fixed rate. However, these do not investigate the performance across channel conditions with varying delay/Doppler spreads and code rates. In [4], [20], maximum ratio combining/full complexity minimum mean square error (FC-MMSE)-based turbo equalization schemes for OTFS are proposed; however, their impact on coded performance is not analyzed. Moreover, existing analytical results evaluate diversity [8], [9], [21] and IS for OTFS in the DD domain and for OFDM in the TF domain [11], which does not enable fair comparison. A common TF-domain analysis is required. Table I summarizes the focus of this paper in the context of existing literature.

We develop a unified framework to analyze and compare OFDM and OTFS under identical equalizers across diverse channel conditions, accounting for SS and IS, and in both uncoded and coded transmissions.

B. Contributions and Takeaways

We make the following key theoretical contributions:

1) We develop a TF-domain analytical model that captures SS and IS in both OFDM and OTFS, revealing their distinct characteristics and the intrinsic effects they induce. Specifically, *i)* the SS structure gives rise to differing time and frequency diversities in OFDM and OTFS. We examine how these diversities are induced by the multipath delay and Doppler components (see Theorem 1, (22), and (23) in Sec. III-A); *ii)* the IS structure leads to either concentrated or fully spread interference in the TF domain (see Theorem 2 in Sec. III-B); and *iii)* the SS and IS power levels (see Sec. III-C) determine the signal-to-interference ratio (SIR). We also analyze how these depend on $\tau_{\max}$ and $\nu_{\max}$ of the channel. These effects ultimately govern the waveform's performance.

2) We consider four channel conditions–flat-fading, purely delay-spread, purely Doppler-spread, and DD-spread. For each case, we derive explicit expressions for the SS and IS, and show how they determine the performance of a waveform in different channel conditions (see Sec IV).

3) We analyze how the SS-IS effects manifest in data detection by considering two representative equalizers: an interference-agnostic equalizer (the 1-tap equalizer, see Sec. V-A) and an interference-suppressing equalizer (the FC-MMSE equalizer, see Sec. V-B). We derive the post-equalization SINR to relate the SS/IS to the BER (see (41), (43) in Sec. V). For each equalizer, we then explicitly study (i) the relative performance of OFDM and OTFS, (ii) the performance trends across different channel conditions, and (iii) the impact of increasing $\tau_{\max}$ and $\nu_{\max}$ on the TF diversity and hence the performance.

4) We conduct a detailed analysis of the source of SS in uncoded OTFS, which is absent in OFDM. We further show that OTFS and OFDM can be viewed as two operating points on a broader spreading-localization continuum, a perspective not previously explored (see Sec. VI-A).

5) We extend the analysis to coded communications and show how channel coding enables OFDM to obtain similar SS (thus TF diversity). This allows OFDM to achieve performance comparable to OTFS (see Sec. VI-B).

6) We develop a novel low-complexity variational Bayesian-based log-likelihood ratio (VB-LLR) algorithm for reliable LLR computation, and investigate how the quality of the resulting LLRs and the code rates affect the performance of OFDM and OTFS (see Sec. VI-C).

Our empirical results corroborate the theoretical analysis and reveal the following key insights:

- In uncoded transmission, OFDM and OTFS perform comparably in flat-fading channels, while OTFS outperforms OFDM in harsher channel conditions.

- For OFDM, and with a 1-tap equalizer, flat-fading and purely delay-spread channels provide superior performance compared to purely Doppler-spread and DD-spread channels. However, when the FC-MMSE equalizer is employed, the performance in purely Doppler-spread and DD-spread channels improves significantly and exceeds that of flat-fading and purely delay-spread channels.
- Under the 1-tap equalizer, OTFS performance is governed by the TF diversity–SIR tradeoff, while the FC-MMSE equalizer provides an equalizer gain in addition to extracting the TF diversity. As a consequence, performance is best under DD-spread channels, followed by purely Doppler-, purely delay-spread, and flat-fading channels.
- OFDM performance remains unchanged with increasing $\tau_{\max}$, whereas OTFS improves up to a saturation point.
- With increasing $\nu_{\max}$, OFDM degrades under the 1-tap but improves slowly under FC-MMSE; OTFS exhibits an initial improvement and subsequent degradation under 1-tap, but improves monotonically under FC-MMSE.
- VB-LLR performs best among the considered equalizers, although, in uncoded communications, the relative performance of OFDM vs. OTFS remains similar to the FC-MMSE.
- In coded transmission, OFDM becomes comparable to OTFS at low (1-tap/FC-MMSE) and moderate (VB-LLR) code rates, and can even outperform OTFS at lower rates. This sharp contrast in the behavior of the waveforms with/without coding is due to channel coding, which enables the extraction of time-frequency diversity in the channel, especially when VB-LLR is used to obtain high-quality soft symbol estimates.
- In coded transmission, both waveforms' performance improves with $\tau_{\max}$ under all equalizers. As $\nu_{\max}$ increases, they exhibit an extended improvement region under the 1-tap before degrading, whereas the performance improves monotonically under the VB-LLR equalizer.

Notation: $(\cdot)^T$, $(\cdot)^H$, $(\cdot)^*$, $\mathrm{Tr}(\cdot)$, $\|\cdot\|$, $\|\cdot\|_{\mathrm{F}}$, $\otimes$, $\odot$, $\lfloor\cdot\rfloor$, $\mathrm{vec}(\cdot)$, $\mathbf{1}_N$ represent the transpose, Hermitian, complex conjugate, trace, ℓ_2 norm, Frobenius norm, Kronecker product, Hadamard product, floor, vectorization operations, and the N-dimensional vector of all ones. $\mathbf{x}_{\neq i}$, $\mathrm{diag}[\cdot]$, $\mathcal{CN}(\boldsymbol{\mu}, \boldsymbol{\Sigma})$, and $\mathcal{U}(\varphi_1, \varphi_2)$ denote the vector $\mathbf{x}$ after deleting the ith entry, an operator returning a vector of diagonal entries for a matrix and a diagonal matrix for a vector, a circularly symmetric complex Gaussian distribution with mean $\boldsymbol{\mu}$ and covariance $\boldsymbol{\Sigma}$, and a uniform distribution on $[\varphi_1, \varphi_2]$.

II. System Model

We consider the transmission of a data signal using OFDM/OTFS waveforms occupying a bandwidth of B Hz and a time-duration of T_{d} s, as shown in Fig. 1. In this section, we present the input–output relationships for these waveforms. For fair comparison, we consider cyclic prefix (CP)-OFDM and CP-OTFS [4], [24] in our system model.

A. OFDM Modulation

Consider an OFDM system with M subcarriers and a subcarrier spacing of $\Delta f = B/M$. The OFDM symbol duration is $T = 1/\Delta f$, and the total duration T_{d} can accommodate $N = \lfloor \frac{T_{\mathrm{d}}}{T+T_{\mathsf{CP}}} \rfloor$ symbols, where T_{CP} denotes the CP duration associated with each symbol. At the transmitter side, the OFDM modulator is represented by the inner block in Fig. 1. The data symbols are mapped onto the TF domain in a two-dimensional (2D) fashion, $\mathbf{X}_{\mathrm{TF}} \in \mathbb{C}^{M\times N}$. An M-point inverse discrete Fourier transform (IDFT) followed by pulse-shaping with a filter $g_{\mathrm{tx}}(t)$ for $t \in [0, T]$, and a parallel-to-serial conversion, yields the time-domain signal vector as

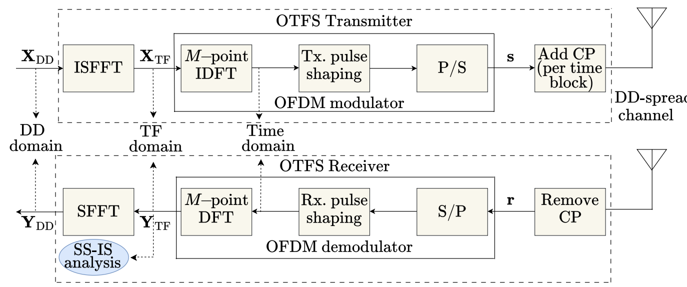

Fig. 1: Transmitter and receiver blocks for OFDM and OTFS.

$$\mathbf{s}_{\mathrm{F}} = (\mathbf{I}_N \otimes \mathbf{G}_{\mathrm{tx}} \mathbf{F}_M^H)\mathbf{x}_{\mathrm{TF}} = \mathbf{G}_{\mathrm{F}} \mathbf{x}_{\mathrm{TF}}, \tag{1}$$

where $\mathbf{G}_{\mathrm{tx}} = \mathrm{diag}[g_{\mathrm{tx}}(0), g_{\mathrm{tx}}(\frac{T}{M}), \ldots, g_{\mathrm{tx}}(\frac{(M-1)T}{M})] \in \mathbb{C}^{M\times M}$, $\mathbf{F}_M \in \mathbb{C}^{M\times M}$ and $\mathbf{I}_N \in \mathbb{C}^{N\times N}$ denote the unitary DFT and identity matrices, respectively, and $\mathbf{x}_{\mathrm{TF}} = \mathrm{vec}(\mathbf{X}_{\mathrm{TF}}) \in \mathbb{C}^{MN}$. We assume a rectangular pulse shaping filter, i.e., $\mathbf{G}_{\mathrm{tx}} = \mathbf{I}_M$, and thus, the OFDM modulator matrix is given by $\mathbf{G}_{\mathrm{F}} \triangleq \mathbf{I}_N \otimes \mathbf{F}_M^H \in \mathbb{C}^{MN\times MN}$ [4].

B. OTFS Transmitter

The OTFS transmitter block consists of an inverse symplectic finite Fourier transform (ISFFT) followed by an OFDM modulator, as shown in the outer box on the transmitter side of Fig. 1. For $M \times N$ OTFS system, we mount the data symbols on the 2D DD domain, $\mathbf{X}_{\mathrm{DD}} \in \mathbb{C}^{M\times N}$, with delay and Doppler bins $\frac{l}{M\Delta f}$ and $\frac{k}{NT}$ for $l \in \{0, \ldots, M-1\}$ and $k \in \{0, \ldots, N-1\}$, respectively. The symbols are then converted to the TF domain using the ISFFT operation as

$$\mathbf{X}_{\mathrm{TF}} = \mathbf{F}_M \mathbf{X}_{\mathrm{DD}} \mathbf{F}_N^H. \tag{2}$$

The vectorized version of the TF domain symbols can be represented as

$$\mathbf{x}_{\mathrm{TF}} \triangleq \mathrm{vec}(\mathbf{X}_{\mathrm{TF}}) = (\mathbf{F}_N^H \otimes \mathbf{F}_M)\mathbf{x}_{\mathrm{DD}} = \mathbf{G}_{\mathrm{T}} \mathbf{x}_{\mathrm{DD}}, \tag{3}$$

where the OTFS pre-processing matrix is denoted by

$$\mathbf{G}_{\mathrm{T}} \triangleq \mathbf{F}_N^H \otimes \mathbf{F}_M \in \mathbb{C}^{MN\times MN}, \tag{4}$$

and $\mathbf{x}_{\mathrm{DD}} = \mathrm{vec}(\mathbf{X}_{\mathrm{DD}}) \in \mathbb{C}^{MN}$. Then the symbols go through the OFDM modulator, and we get the time domain signal vector, similar to (1), as [4]

$$\mathbf{s}_{\mathrm{T}} = \mathbf{G}_{\mathrm{F}} \mathbf{G}_{\mathrm{T}} \mathbf{x}_{\mathrm{DD}}. \tag{5}$$

We then append a CP of $\lceil T_{\mathsf{CP}} B \rceil$ samples in the time domain to each time block of the OTFS frame. Thus, the total number of data symbols transmitted over the bandwidth B Hz and time duration T_{d} s is the same for OFDM and OTFS.

C. DD-Spread Channels

We consider a DD-spread channel, where the received signal corresponding to the input $s(t)$ is given by

$$r(t) = \sum_{p=1}^{P} h_p s(t-\tau_p) e^{j2\pi\nu_p t} + w(t). \tag{6}$$

Here, P denotes the number of discrete scattering paths, (h_p, τ_p, ν_p) denote the complex channel gain, delay, and Doppler shift of the pth path, and $w(t)$ represents the complex AWGN. Further, $\tau_p \in [0, \tau_{\max}]$ and $\nu_p \in [-\nu_{\max}, \nu_{\max}]$, where $\tau_{\max}$ and $\nu_{\max}$ denote the delay and Doppler spreads of the channel, respectively. Thus, τ_p and ν_p can take fractional values. The signal $s(t)$ corresponds to the continuous-time version of $\mathbf{s}$ (as in (1) and (5)) after adding the CP, as illustrated in Fig. 1. We also assume that the CP duration satisfies $T_{\mathsf{CP}} \geq \tau_{\max}$. At the receiver, after CP removal, the signal can be expressed in matrix-vector form as [24], [25]

$$\mathbf{r} = \mathbf{H}^t \mathbf{s} + \mathbf{w}^t. \tag{7}$$

The time-domain channel matrix $\mathbf{H}^t \in \mathbb{C}^{MN \times MN}$ is given by

$$\mathbf{H}^t \triangleq \sum_{n=0}^{N-1} (\mathbf{e}_n \mathbf{e}_n^T) \otimes \Big(\sum_{p=1}^{P} h_p \mathbf{F}_M^H \mathbf{\Gamma}_p \mathbf{F}_M \mathbf{\Delta}_{p,n} \Big), \tag{8}$$

where $\mathbf{e}_n$ is the nth canonical basis vector in $\mathbb{C}^N$, with

$$\mathbf{\Gamma}_p = \mathrm{diag}(\boldsymbol{\gamma}_p) \text{ and } \mathbf{\Delta}_{p,n} = \mathrm{diag}(\mathbf{d}_{p,n}). \tag{9}$$

Here, $\boldsymbol{\gamma}_p = [1, e^{-j2\pi\Delta f \tau_p}, \ldots, e^{-j2\pi(M-1)\Delta f \tau_p}]^T \in \mathbb{C}^M$ and $\mathbf{d}_{p,n} = e^{j2\pi n (T+T_{\mathsf{CP}})\nu_p} [1, e^{j2\pi \frac{T}{M}\nu_p}, \ldots, e^{j2\pi \frac{(M-1)T}{M}\nu_p}]^T \in \mathbb{C}^M$. The channel matrix $\mathbf{H}^t$ is a time-domain representation of the DD-spread channel, which transforms the time-domain transmitted signal $\mathbf{s}$ into the time-domain received signal $\mathbf{r}$. Finally, the time-domain AWGN: $\mathbf{w}^t \sim \mathcal{CN}(\mathbf{0}, \sigma^2 \mathbf{I}_{MN}) \in \mathbb{C}^{MN}$.

D. OFDM Demodulator and OTFS Receiver

The OFDM demodulator and OTFS receiver are shown in inner and outer blocks of the receiver side in Fig. 1, respectively. The received time-domain signal in (7) is processed by the OFDM demodulator, which inverts the operations of the OFDM modulator to recover the TF-symbol matrix

$$\mathbf{Y}_{\mathrm{TF}} = \mathbf{F}_M \mathbf{G}_{\mathrm{rx}} \mathrm{vec}^{-1}(\mathbf{r}), \tag{10}$$

where $\mathbf{G}_{\mathrm{rx}}$ denotes the receiver pulse-shaping filter (assumed to be the same as $\mathbf{G}_{\mathrm{tx}} = \mathbf{I}_M$), and $\mathrm{vec}^{-1}(\cdot)$ converts an $MN \times 1$ vector into an $M \times N$ matrix. The vectorized TF-domain received signal can be written as

$$\begin{aligned} \mathbf{y}_{\mathrm{TF}} \triangleq \mathrm{vec}(\mathbf{Y}_{\mathrm{TF}}) &= \mathbf{G}_{\mathrm{F}}^H \mathbf{H}^t \mathbf{G}_{\mathrm{F}} \mathbf{x}_{\mathrm{TF}} + \mathbf{G}_{\mathrm{F}}^H \mathbf{w}^t \\ &= \mathbf{H}_{\mathrm{TF}} \mathbf{x}_{\mathrm{TF}} + \mathbf{w}_{\mathrm{TF}}, \end{aligned} \tag{11}$$

where the TF-domain channel $\mathbf{H}_{\mathrm{TF}} \in \mathbb{C}^{MN \times MN}$ is given by

$$\mathbf{H}_{\mathrm{TF}} \triangleq \mathbf{G}_{\mathrm{F}}^H \mathbf{H}^t \mathbf{G}_{\mathrm{F}} = \sum_{n=0}^{N-1} (\mathbf{e}_n \mathbf{e}_n^T) \otimes \Big(\sum_{p=1}^{P} h_p \mathbf{\Gamma}_p \mathbf{F}_M \mathbf{\Delta}_{p,n} \mathbf{F}_M^H \Big). \tag{12}$$

The transformed noise term is $\mathbf{w}_{\mathrm{TF}} \triangleq \mathbf{G}_{\mathrm{F}}^H \mathbf{w}^t \sim \mathcal{CN}(\mathbf{0}, \sigma^2 \mathbf{I}_{MN})$. For OTFS, SFFT transforms the TF-domain vector into the DD-domain vector as

$$\mathbf{y}_{\mathrm{DD}} = \mathbf{G}_{\mathrm{T}}^H \mathbf{y}_{\mathrm{TF}} + \mathbf{G}_{\mathrm{T}}^H \mathbf{w}_{\mathrm{TF}} = \mathbf{H}_{\mathrm{DD}} \mathbf{x}_{\mathrm{DD}} + \mathbf{w}_{\mathrm{DD}}, \tag{13}$$

where, using (4), the DD-domain channel $\mathbf{H}_{\mathrm{DD}} \triangleq \mathbf{G}_{\mathrm{T}}^H \mathbf{H}_{\mathrm{TF}} \mathbf{G}_{\mathrm{T}} \in \mathbb{C}^{MN \times MN}$ is given by

$$\mathbf{H}_{\mathrm{DD}} = \sum_{n=0}^{N-1} \Big([\mathbf{F}_N]_{(:,n)} [\mathbf{F}_N]_{(:,n)}^H \Big) \otimes \Big(\sum_{p=1}^{P} h_p \mathbf{F}_M^H \mathbf{\Gamma}_p \mathbf{F}_M \mathbf{\Delta}_{p,n} \Big) \tag{14}$$

and $\mathbf{w}_{\mathrm{DD}} \triangleq \mathbf{G}_{\mathrm{DD}}^H \mathbf{w}_{\mathrm{TF}} \sim \mathcal{CN}(\mathbf{0}, \sigma^2 \mathbf{I}_{MN})$.

III. Symbol- and Interference-Spreading (SS & IS)

Let the transmitted data symbols be denoted by $\mathbf{x} \in \mathbb{C}^{MN}$, which are mapped to the TF domain in OFDM ($\mathbf{x}_{\mathrm{TF}} = \mathbf{x}$) and to the DD domain in OTFS ($\mathbf{x}_{\mathrm{DD}} = \mathbf{x}$). From (11), the noise-free TF-domain received signals for OFDM and OTFS can be respectively written as

$$\mathbf{y}_{\mathrm{F}} = \mathbf{H}_{\mathrm{TF}} \mathbf{x} \text{ and } \mathbf{y}_{\mathrm{T}} = \mathbf{H}_{\mathrm{TF}} \mathbf{G}_{\mathrm{T}} \mathbf{x}. \tag{15}$$

Thus, in OFDM, each symbol in $\mathbf{x}$ interacts only with its corresponding column of $\mathbf{H}_{\mathrm{TF}}$, i.e., the ith symbol is influenced solely by the ith column of $\mathbf{H}_{\mathrm{TF}}$ for $i \in \{0, \ldots, MN-1\}$. In contrast, for OTFS, due to the presence of $\mathbf{G}_{\mathrm{T}}$, each symbol interacts with all columns of $\mathbf{H}_{\mathrm{TF}}$, implying that the ith symbol interacts with the entire TF channel. These differences motivate the notions of SS and IS across the TF domain.

To quantify the SS and IS caused by a single symbol, we consider a unit excitation at the i_0th symbol position, i.e., $\mathbf{x} = \mathbf{e}_{i_0}$, where $\mathbf{e}_{i_0}$ is the i_0th canonical basis vector in $\mathbb{C}^{MN}$. For OFDM, this corresponds to the (n_0, m_0)th TF bin, where $m_0 = \mod(i_0, M)$, $n_0 = (i_0 - m_0)/M$. For OTFS, it corresponds to the (k_0, l_0)th DD bin, where $l_0 = \mod(i_0, M)$, $k_0 = (i_0 - l_0)/M$. Then, $\mathbf{y}_{\mathrm{F}}$ and $\mathbf{y}_{\mathrm{T}}$ become

$$\mathbf{y}_{\mathrm{F}} = \mathrm{diag}(\mathbf{H}_{\mathrm{TF}}) \odot \mathbf{e}_{i_0} + (\mathbf{H}_{\mathrm{TF}} \mathbf{e}_{i_0} - \mathrm{diag}(\mathbf{H}_{\mathrm{TF}}) \odot \mathbf{e}_{i_0}), \tag{16}$$

$$\begin{aligned} \mathbf{y}_{\mathrm{T}} &= \mathrm{diag}(\mathbf{H}_{\mathrm{TF}}) \odot [\mathbf{G}_{\mathrm{T}} \mathbf{e}_{i_0}] \\ &\quad + (\mathbf{H}_{\mathrm{TF}} \mathbf{G}_{\mathrm{T}} \mathbf{e}_{i_0} - \mathrm{diag}(\mathbf{H}_{\mathrm{TF}}) \odot [\mathbf{G}_{\mathrm{T}} \mathbf{e}_{i_0}]). \end{aligned} \tag{17}$$

Note that $\mathbf{y}_{\mathrm{F}}$ and $\mathbf{y}_{\mathrm{T}}$ are in the TF-domain. In each expression, we interpret the first term as the SS of the i_0th symbol across the TF domain, and the second term as the IS caused by that symbol on all TF bins other than the (n_0, m_0)th bin. This is because, in OFDM, the transmitter intends to place the i_0th symbol in the corresponding TF bin, but the doubly-dispersive channel leaks its energy into other bins, creating interference with symbols placed on all other bins. In OTFS, the precoder $\mathbf{G}_T$ deliberately spreads the i_0th symbol across the TF bins, and the channel then introduces additional unintended spreading captured by the second term, which causes interference in all TF bins. In the sequel, we will show that these distinct SS and IS characteristics ultimately determine their performance.

A. Effects of SS Structure

From (16) and (17), we define the SS power matrices $\mathbf{P}^S \in \mathbb{C}^{M \times N}$ for OFDM and OTFS as

$$\mathbf{P}_{\mathrm{F}}^S = \left| [\mathbf{H}_{\mathrm{TF}}]_{(i_0, i_0)} \right|^2 \mathbf{e}_{m_0} \mathbf{e}_{n_0}^T, \tag{18}$$

$$\mathbf{P}_{\mathrm{T}}^{S}=\mathrm{vec}^{-1}\left(|\mathrm{diag}(\mathbf{H}_{\mathrm{TF}})\odot[\mathbf{G}_{\mathrm{T}}\mathbf{e}_{i_0}]|^{\bullet 2}\right), \tag{19}$$

where $\mathbf{e}_{m_0}$ and $\mathbf{e}_{n_0}$ denote the m_0th and n_0th canonical basis vectors in dimensions M and N, and $(\cdot)^{\bullet 2}$ indicates element-wise squaring. Hence, the SS powers of both waveforms depend on the delay-Doppler characteristics of $\mathbf{H}_{\mathrm{TF}}$ in (12). The following theorem elucidates the structure of $\mathbf{P}_{\mathrm{F}}^{S}$ and $\mathbf{P}_{\mathrm{T}}^{S}$.

Theorem 1. *In DD-spread channels, the SS power matrices for OFDM and OTFS are given by*

$$\mathbf{P}_{\mathrm{F}}^{S}=\left|\sum_{p=1}^{P}h_p[\boldsymbol{\gamma}_p]_{m_0}(\mathbf{1}_M^T\mathbf{d}_{p,n_0})/M\right|^2\mathbf{e}_{m_0}\mathbf{e}_{n_0}^T, \tag{20}$$

$$\mathbf{P}_{\mathrm{T}}^{S}=\frac{1}{MN}\left|\sum_{p=1}^{P}h_p\boldsymbol{\gamma}_p\widetilde{\mathbf{d}}_p^T\right|^{\bullet 2}, \tag{21}$$

where $\mathbf{d}_{p,n_0}$ *is as defined after* (9) *and* $\widetilde{\mathbf{d}}_p=\frac{1}{M}[\mathbf{1}_M^T\mathbf{d}_{p,0},\ldots,\mathbf{1}_M^T\mathbf{d}_{p,N-1}]^T\in\mathbb{C}^N$.

Proof. From (12), we have

$$[\mathbf{H}_{\mathrm{F}}]_{(i_0,i_0)}=\mathbf{e}_{i_0}^T\mathbf{H}_{\mathrm{TF}}\mathbf{e}_{i_0}=(\mathbf{e}_{n_0}\otimes\mathbf{e}_{m_0})^T\mathbf{H}_{\mathrm{TF}}(\mathbf{e}_{n_0}\otimes\mathbf{e}_{m_0})$$
$$=\sum_{p=1}^{P}h_p\mathbf{e}_{m_0}^T\boldsymbol{\Gamma}_p\mathbf{F}_M\boldsymbol{\Delta}_{p,n_0}\mathbf{F}_M^H\mathbf{e}_{m_0}=\sum_{p=1}^{P}\frac{h_p[\boldsymbol{\gamma}_p]_{m_0}(\mathbf{1}_M^T\mathbf{d}_{p,n_0})}{M}.$$

Substituting the above into (18), we obtain the OFDM SS power as (20). Similarly, from (12), with some algebra, the diagonal of $\mathbf{H}_{\mathrm{TF}}$ is expressed as $\mathrm{diag}(\mathbf{H}_{\mathrm{TF}})=\sum_{p=1}^{P}h_p(\widetilde{\mathbf{d}}_p\otimes\boldsymbol{\gamma}_p)$. From (4), $|\mathbf{G}_{\mathrm{T}}\mathbf{e}_{i_0}|=\frac{1}{\sqrt{MN}}\mathbf{1}_{MN}$. Substituting these into (19), we obtain OTFS SS power as (21). ■

Equations (20) and (21) reveal how each waveform utilizes the TF-domain resources. In OFDM, from (20), we see that the i_0th transmitted symbol remains localized on the (n_0,m_0)th TF bin of the received signal. In contrast, from (21), the i_0th symbol is spread across the entire TF domain in OTFS: it experiences different channel gains across frequency depending on the *delay-effect values* $\boldsymbol{\gamma}_p$ and across time depending on the *Doppler-effect values* $\widetilde{\mathbf{d}}_p$. Also, while the SS in OFDM depends only on the m_0th entry of $\boldsymbol{\gamma}_p$ and n_0th entry of $\widetilde{\mathbf{d}}_p$, the SS in OTFS depends on the entire vectors $\boldsymbol{\gamma}_p$ and $\widetilde{\mathbf{d}}_p$. In general, a waveform that achieves greater SS diversity offers improved robustness to fading. In the subsequent sections, we examine in detail how OTFS leverages the delay and Doppler components of the multipath channel to achieve frequency and time diversity, respectively, through its SS structure.

1) Frequency diversity of OTFS: The SS matrix $\mathbf{P}_{\mathrm{T}}^{S}$ captures the spreading of the i_0th transmitted symbol in OTFS across the $M\times N$ TF-bins. In particular, the n^*th column of $\mathbf{P}_{\mathrm{T}}^{S}$ shows the *frequency-domain spreading* within the n^*th time block. From (21),

$$[\mathbf{P}_{\mathrm{T}}^{S}]_{(:,n^*)}=\frac{1}{MN}\left|\sum_{p=1}^{P}h_p\boldsymbol{\gamma}_p[\widetilde{\mathbf{d}}_p]_{n^*}\right|^{\bullet 2}=\frac{1}{MN}\left|\boldsymbol{\Gamma}\mathbf{h}_{\mathbf{d}}\right|^{\bullet 2}, \tag{22}$$

where $\mathbf{h}_{\mathbf{d}}=[h_1[\widetilde{\mathbf{d}}_1]_{n^*},\ldots,h_P[\widetilde{\mathbf{d}}_P]_{n^*}]^T\in\mathbb{C}^P$. The matrix $\boldsymbol{\Gamma}=[\boldsymbol{\gamma}_1,\ldots,\boldsymbol{\gamma}_P]\in\mathbb{C}^{M\times P}$ contains the delay-components of the multipath channel, so that each row in $\boldsymbol{\Gamma}$ represents a *spectral projection* of $\mathbf{h}_{\mathbf{d}}$. As we move across different entries of $[\mathbf{P}_{\mathrm{T}}^{S}]_{(:,n^*)}$, the variations arise solely from different rows of $\boldsymbol{\Gamma}$. Consequently, the effective frequency diversity is governed by the number of independent spectral projections, given by $\mathrm{rank}(\boldsymbol{\Gamma})$, which is at most P (assuming $P\leq M$). Moreover, delay components are *resolvable* when they are separated by at least $1/(M\Delta f)=1/B$, since $|\boldsymbol{\gamma}_q^H\boldsymbol{\gamma}_p|\propto|\mathrm{sinc}(M\Delta f(\tau_q-\tau_p))|\approx 0$ for $|\tau_q-\tau_p|\geq 1/B$, $\forall p,q\in[P]$ and $p\neq q$. If two delay components are not resolvable, they induce highly correlated channel effects in purely delay-spread channels ($\nu_p=0,\forall p$). As $\tau_p\in[0,\tau_{\max}]$, the maximum number of resolvable delay components over bandwidth $B=M\Delta f$ is approximately $\lfloor\tau_{\max}B\rfloor+1$. Therefore, the number of effective independent spectral projections is $D_{\mathrm{freq}}=\min(P,\lfloor\tau_{\max}B\rfloor+1)$.

Now, in purely delay-spread channels, as $\tau_{\max}$ increases from zero, the number of resolvable delay components increases (since they are drawn from $\mathcal{U}[0,\tau_{\max}]$.) In turn, the achievable frequency diversity increases. Since the maximum number of independent components is fundamentally limited by P, the diversity order saturates once this limit is reached. Thus, to achieve the maximum frequency diversity, it is necessary that the number of channel paths must satisfy $P\leq\lfloor\tau_{\max}B\rfloor+1$, which implies $\tau_{\max}\geq(P-1)/B$.

2) Time diversity of OTFS: The m^*th row of $\mathbf{P}_{\mathrm{T}}^{S}$ shows the *time-domain spreading* of the transmitted symbol within the m^*th subcarrier. From (21),

$$[\mathbf{P}_{\mathrm{T}}^{S}]_{(m^*,:)}=\frac{1}{MN}\left|\sum_{p=1}^{P}h_p[\boldsymbol{\gamma}_p]_{m^*}\widetilde{\mathbf{d}}_p^T\right|^{\bullet 2}=\frac{1}{MN}\left|\mathbf{h}_{\boldsymbol{\gamma}}^T\widetilde{\mathbf{D}}\right|^{\bullet 2}, \tag{23}$$

where $\mathbf{h}_{\boldsymbol{\gamma}}=[h_1[\boldsymbol{\gamma}_1]_{m^*},\ldots,h_P[\boldsymbol{\gamma}_P]_{m^*}]^T\in\mathbb{C}^P$. The matrix $\widetilde{\mathbf{D}}=[\widetilde{\mathbf{d}}_1,\ldots,\widetilde{\mathbf{d}}_P]^T\in\mathbb{C}^{P\times N}$ contains the Doppler-components of the multipath channel, with each column representing a temporal projection of the channel. As we move across different entries of $[\mathbf{P}_{\mathrm{T}}^{S}]_{(m^*,:)}$, the variations arise solely from different columns of $\widetilde{\mathbf{D}}$. Consequently, the effective time diversity is governed by the number of independent temporal projections, given by $\mathrm{rank}(\widetilde{\mathbf{D}})$, of which there are at most P (assuming $P\leq N$). Doppler components are *resolvable* when separated by at least $1/(N(T+T_{\mathsf{CP}}))$, since $|\widetilde{\mathbf{d}}_q^H\widetilde{\mathbf{d}}_p|\propto\mathrm{sinc}(N(T+T_{\mathsf{CP}})(\nu_q-\nu_p))|\approx 0$ for $|\nu_q-\nu_p|\geq 1/(N(T+T_{\mathsf{CP}}))$ and $p\neq q$. If two Doppler components are not resolvable, their separation is $\leq 1/N(T+T_{\mathsf{CP}})$, and they induce highly correlated channel effects in purely Doppler-spread channels ($\tau_p=0,\forall p$). As $\nu_p\in[-\nu_{\max},\nu_{\max}]$, the number of resolvable Doppler components over the duration $T_{\mathrm{d}}=N(T+T_{\mathsf{CP}})$ is approximately $\lfloor 2\nu_{\max}T_{\mathrm{d}}\rfloor+1$. Therefore, the number of effective temporal projections is $D_{\mathrm{time}}=\min(P,\lfloor 2\nu_{\max}T_{\mathrm{d}}\rfloor+1)$.

Now, in purely Doppler-spread channels, as $\nu_{\max}$ increases, the number of resolvable Doppler components (and hence the achievable time diversity) increases. Since the maximum number of independent channel components is P, the time diversity saturates once this limit is reached. Thus, to achieve the maximum time diversity, the condition $\lfloor 2\nu_{\max}T_{\mathrm{d}}\rfloor+1\geq P$ must hold, which yields $\nu_{\max}\geq(P-1)/(2T_{\mathrm{d}})$.

B. Effects of IS Structure

From (16) and (17), we define the IS power matrices $\mathbf{P}^I \in \mathbb{C}^{M\times N}$ for OFDM and OTFS as

$$\mathbf{P}_{\mathrm{F}}^I = \mathrm{vec}^{-1}\left(|\mathbf{H}_{\mathrm{TF}}\mathbf{e}_{i_0} - \mathrm{diag}(\mathbf{H}_{\mathrm{TF}}) \odot \mathbf{e}_{i_0}|^{\bullet 2}\right), \tag{24}$$

$$\mathbf{P}_{\mathrm{T}}^I = \mathrm{vec}^{-1}\left(|\mathbf{H}_{\mathrm{TF}}\mathbf{G}_{\mathrm{T}}\mathbf{e}_{i_0} - \mathrm{diag}(\mathbf{H}_{\mathrm{TF}})\odot[\mathbf{G}_{\mathrm{T}}\mathbf{e}_{i_0}]|^{\bullet 2}\right). \tag{25}$$

The following theorem elucidates the structure of $\mathbf{P}_{\mathrm{F}}^I$ and $\mathbf{P}_{\mathrm{T}}^I$.

Theorem 2. *In DD-spread channels, the IS power for OFDM and OTFS is given by*

$$\mathbf{P}_{\mathrm{F}}^I = \left|\sum_{p=1}^{P} h_p\left(\left(\boldsymbol{\gamma}_p \odot \left(\mathbf{F}_M\left(\mathbf{d}_{p,n_0} \odot [\mathbf{F}_M]^H_{(m_0,:)}\right)\right)\right) - \frac{1}{M}[\boldsymbol{\gamma}_p]_{m_0}(\mathbf{1}_M^T\mathbf{d}_{p,n_0})\mathbf{e}_{m_0}\right)\right|^{\bullet 2}\mathbf{e}_{n_0}^T, \tag{26}$$

$$\mathbf{P}_{\mathrm{T}}^I = \frac{1}{MN}\left|\sum_{p=1}^{P} h_p\boldsymbol{\gamma}_p\left(\widetilde{\mathbf{d}}_{p,m_0} - \widetilde{\mathbf{d}}_p\right)^T\right|^{\bullet 2}, \tag{27}$$

where $\widetilde{\mathbf{d}}_{p,m_0} = [[\mathbf{d}_{p,0}]_{m_0}, \ldots, [\mathbf{d}_{p,N-1}]_{m_0}]^T \in \mathbb{C}^N$.

Proof. From (12), we can write

$$\begin{aligned}\mathbf{H}_{\mathrm{TF}}\mathbf{e}_{i_0} &= \mathbf{H}_{\mathrm{TF}}(\mathbf{e}_{n_0} \otimes \mathbf{e}_{m_0}) \\ &= \sum_{p=1}^{P} h_p\mathbf{e}_{n_0} \otimes \left(\boldsymbol{\gamma}_p \odot \left(\mathbf{F}_M\left(\mathbf{d}_{p,n_0} \odot [\mathbf{F}_M]^H_{(m_0,:)}\right)\right)\right).\end{aligned} \tag{28}$$

From (4), $\mathbf{G}_{\mathrm{T}}\mathbf{e}_{i_0} = [\mathbf{F}_N]^H_{(n_0,:)} \otimes [\mathbf{F}_M]_{(:,m_0)}$. Substituting these into (24) and (25) yields (26) and (27), respectively. ∎

From (26), we see that IS caused by the i_0th symbol in OFDM appears only along the frequency axis within the n_0th time block, whereas (27) shows that in OTFS the IS[1] spreads over the entire TF-domain. The concentrated IS in OFDM can be less detrimental than the widely spread IS in OTFS; this effect is examined in Sec. V. Note that, in DD-spread channels ($\tau_{\max} > 0, \nu_{\max} > 0$), increasing $\tau_{\max}$ or $\nu_{\max}$ does not alter the IS structure (concentrated/fully spread) in OFDM and OTFS. So far, we have elucidated the SS and IS structures and their impact on the performance. We now investigate how the power levels of SS and IS influence the performance.

C. Impact of SS and IS Power Levels

We examine the effect of SS-IS power level in two ways: 1) how they determine the relative performance of OFDM and OTFS, i.e., whether the two waveforms exhibit different SS or IS power levels, and, 2) how they govern the performance of a given waveform across different channel conditions (characterized by $\tau_{\max}$ and $\nu_{\max}$).

[1]In OFDM, the i_0th symbol is placed in the TF domain, and $\mathbf{P}_{\mathrm{F}}^I$ represents the resulting ICI/ISI on other TF bins. In OTFS, the symbol is placed in the DD domain, and $\mathbf{P}_{\mathrm{T}}^I$ captures its induced TF-domain interference, which does not correspond directly to conventional ICI/ISI.

1) Relative performance of OFDM and OTFS: The SS expressions in (20), (21) and IS expressions in (26), (27) correspond to a unit excitation at the i_0th symbol. While these expressions may appear to indicate different SS and IS power levels for OFDM and OTFS, the total SS (and IS) power summed over all TF bins (n,m) and all symbol excitations (n_0,m_0) is the *same for both waveforms*, i.e., $\sum_{i=0}^{MN-1}\|\mathrm{diag}(\mathbf{H}_{\mathrm{TF}}) \odot \mathbf{e}_i\|^2 = \sum_{i=0}^{MN-1}\|\mathrm{diag}(\mathbf{H}_{\mathrm{TF}}) \odot [\mathbf{G}_{\mathrm{T}}\mathbf{e}_i]\|^2$, and $\sum_{i=0}^{MN-1}\|\mathbf{H}_{\mathrm{TF}}\mathbf{e}_i - \mathrm{diag}(\mathbf{H}_{\mathrm{TF}}) \odot \mathbf{e}_i\|^2 = \sum_{i=0}^{MN-1}\|\mathbf{H}_{\mathrm{TF}}\mathbf{G}_{\mathrm{T}}\mathbf{e}_i - \mathrm{diag}(\mathbf{H}_{\mathrm{TF}}) \odot [\mathbf{G}_{\mathrm{T}}\mathbf{e}_i]\|^2$. This follows from the unitary nature of the OTFS precoding matrix $\mathbf{G}_{\mathrm{T}}$. This follows from the unitary nature of the OTFS precoding matrix $\mathbf{G}_{\mathrm{T}}$. Thus, OFDM and OTFS exhibit similar SS and IS power levels, and hence the SIR.

2) Effect of $\tau_{\max}$ and $\nu_{\max}$: To examine the effect of $\tau_{\max}$ and $\nu_{\max}$ on SS and IS power levels, we compute the expected SS and IS powers with respect to the channel gain vector $\mathbf{h}$, assuming $h_p \overset{\text{i.i.d.}}{\sim} \mathcal{CN}(0, 1/P)$.

a) Increasing $\tau_{\max}$: The matrices $\mathbb{E}_{\mathbf{h}}[\mathbf{P}_{\mathrm{F}}^S]$, $\mathbb{E}_{\mathbf{h}}[\mathbf{P}_{\mathrm{F}}^I]$, $\mathbb{E}_{\mathbf{h}}[\mathbf{P}_{\mathrm{T}}^S]$, and $\mathbb{E}_{\mathbf{h}}[\mathbf{P}_{\mathrm{T}}^I]$, contain multiplicative terms involving $|\boldsymbol{\gamma}_p|$, where $\boldsymbol{\gamma}_p$ solely depends on the delay parameters. Since $|\boldsymbol{\gamma}_p| = \mathbf{1}_M$ irrespective of $\tau_{\max}$, variations in $\tau_{\max}$ do not influence the expected SS and IS power levels.

b) Increasing $\nu_{\max}$: For OFDM, we can write

$$\mathbb{E}_{\mathbf{h}}[\mathbf{P}_{\mathrm{F}}^S] = (1/P^2)\sum\nolimits_{p=1}^{P} f_\nu(\nu_p)\mathbf{e}_{m_0}\mathbf{e}_{n_0}^T, \tag{29}$$

where $f_\nu(\nu_p) \triangleq \frac{1}{M^2}\frac{\sin^2(\pi T\nu_p)}{\sin^2(\pi T\nu_p/M)}$.The function $f_\nu(\nu_p)$ is periodic with period M/T, achieves its maximum at $\nu_p = 0$, and decreases monotonically with $|\nu_p|$ within the main-lobe region $|\nu_p| < 1/T$. Since the practical OFDM/OTFS system satisfy $\nu_{\max} < \frac{1}{T}$ [7], increasing $\nu_{\max}$ reduces the expected SS power. Similarly, in OTFS, each entry of $|\widetilde{\mathbf{d}}_p|$ decreases with increasing $|\nu_p|$, leading to a reduction in $\mathbb{E}_{\mathbf{h}}[\mathbf{P}_{\mathrm{T}}^S]$. For OFDM, the expected IS power is given by

$$\mathbb{E}_{\mathbf{h}}[\mathbf{P}_{\mathrm{F}}^I] = \frac{1}{P^2}\sum_{p=1}^{P}\left|\mathbf{F}_M\left(\mathbf{d}_{p,n_0} \odot [\mathbf{F}_M]^H_{(m_0,:)}\right) - \frac{1}{M}(\mathbf{1}_M^T\mathbf{d}_p)\right|^{\bullet 2}\mathbf{e}_{n_0}^T, \tag{30}$$

whose (n,m)th entry can be written as $\sum_{p=1}^{P} f_\nu(\frac{m-m_0}{T} - \nu_p)\mathbb{1}_{m\neq m_0, n=n_0}$. Letting $u = m - m_0$, this function is periodic in ν_p with its main lobe centered at $\nu_p = u/T$. Since $|\nu_p| < 1/T$, only the neighboring subcarriers $u = \pm 1$ overlap with the main lobe region. In this overlap region, the interference power increases monotonically with $|\nu_p|$. For OTFS, since $|\widetilde{\mathbf{d}}_{p,m_0}| = \mathbf{1}_N$, the IS behavior is dominated by $|\widetilde{\mathbf{d}}_p|$. As $|\nu_p|$ increases, entries in $|\widetilde{\mathbf{d}}_p|$ decrease, resulting in increased interference power. Thus, increasing $\nu_{\max}$ reduces the SIR for both waveforms, which can impact performance.

In summary, the effects of SS and IS characteristics that determine waveform performance are as follows: *i)* OFDM does not provide diversity through SS, whereas OTFS enables two forms of diversity: (a) frequency diversity, which increases with $\tau_{\max}$, and (b) time diversity, which increases with $\nu_{\max}$. The necessary conditions for achieving the maximum frequency and time diversities are: $\tau_{\max} \geq (P-1)/B$ and $\nu_{\max} \geq (P-1)/(2T_{\mathrm{d}})$, respectively. *ii)* The IS structure in OFDM is concentrated along the frequency axis within a time block, while in OTFS, the interference spreads across the entire TF-domain. *iii)* OFDM and OTFS exhibit identical total SS and IS power levels, hence, the same SIR. However, for both waveforms, $\tau_{\max}$ does not affect the SS/IS power levels, whereas increasing $\nu_{\max}$ reduces the SS power and increases the IS power, thereby reducing the SIR.

How these effects translate into actual performance depends on the equalizer employed and its sensitivity to these effects, and is discussed in Sec. V.

Thus far, we have focused on the SS and IS characteristics of OFDM and OTFS in DD-spread channels. We now extend the analysis to other channel conditions and present TF-domain visualizations of SS and IS in the next section

IV. SS-IS in Different Channel Conditions

We consider four channel conditions based on $\tau_{\max}$ and $\nu_{\max}$: flat-fading ($\tau_{\max}=0, \nu_{\max}=0$), purely delay-spread ($\tau_{\max}>0, \nu_{\max}=0$), purely Doppler-spread ($\tau_{\max}=0, \nu_{\max}>0$), and DD-spread channels ($\tau_{\max}>0, \nu_{\max}>0$). We derive explicit expressions for SS and IS in these channels and analyze the intrinsic characteristics that determine a waveform's performance across different channel conditions.

A. Flat-Fading Channels

This channel can be modeled by a single path ($P=1$) with $\tau_1=\nu_1=0$. From (9), $\boldsymbol{\gamma}_1=\mathbf{d}_{1,n}=\mathbf{1}_M, \forall n$, yielding

$$\mathbf{P}_{\mathrm{F}}^{S}=|h_1|^2\,\mathbf{e}_{m_0}\mathbf{e}_{n_0}^{T}, \quad \mathbf{P}_{\mathrm{F}}^{I}=\mathbf{0}_{M\times N}. \tag{31}$$

$$\mathbf{P}_{\mathrm{T}}^{S}=\frac{1}{MN}|h_1|^2\,\mathbf{1}_{M\times N}, \quad \mathbf{P}_{\mathrm{T}}^{I}=\mathbf{0}_{M\times N}. \tag{32}$$

Thus, both OFDM and OTFS exhibit no interference. In OTFS, the symbol energy is uniformly spread over the entire TF domain with identical gain, but it yields no diversity.

B. Purely Delay-Spread Channels

Here, $\nu_p=0, \mathbf{d}_{p,n}=\mathbf{1}_M, \forall p,n$. The SS-IS powers become

$$\mathbf{P}_{\mathrm{F}}^{S}=\Big|\sum_{p=1}^{P}h_p[\boldsymbol{\gamma}_p]_{m_0}\Big|^2\mathbf{e}_{m_0}\mathbf{e}_{n_0}^{T}, \quad \mathbf{P}_{\mathrm{F}}^{I}=\mathbf{0}_{M\times N} \tag{33}$$

$$\mathbf{P}_{\mathrm{T}}^{S}=\frac{1}{MN}\Big|\sum_{p=1}^{P}h_p\boldsymbol{\gamma}_p\Big|^{\bullet 2}\mathbf{1}_{N}^{T}, \quad \mathbf{P}_{\mathrm{T}}^{I}=\mathbf{0}_{M\times N}. \tag{34}$$

OTFS exhibits frequency diversity via gain variation along the frequency axis, which increases with $\tau_{\max}$ up to nearly $\tau_{\max}=(P-1)/B$ and then saturates (see Sec. III-A1). No interference arises in OFDM/OTFS since $\tau_{\max}\leq T_{\mathrm{CP}}$, and the TF-domain channel becomes diagonal. Moreover, $\tau_{\max}$ has no impact on the SIR for both waveforms.

C. Purely Doppler-Spread Channels

In this case, $\tau_p=0, \boldsymbol{\gamma}_p=\mathbf{1}_M, \forall p$. The SS-IS powers are

$$\mathbf{P}_{\mathrm{F}}^{S}=\Big|\sum_{p=1}^{P}h_p(\mathbf{1}_M^{T}\mathbf{d}_{p,n_0})/M\Big|^2\mathbf{e}_{m_0}\mathbf{e}_{n_0}^{T}, \tag{35}$$

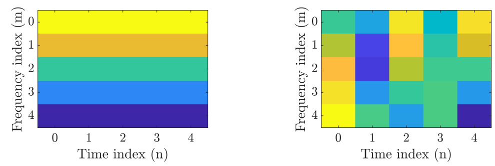

(a) Purely delay-spread channels **(b)** DD-spread channels

Fig. 2: TF-domain SS of OTFS. It provides frequency diversity in delay-spread channels, and time-and-frequency diversity in DD-spread channels.

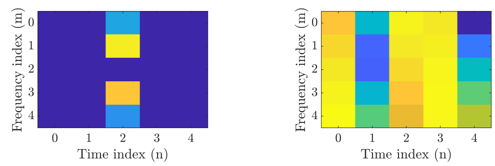

(a) OFDM in purely Doppler/DD **(b)** OTFS in DD-spread channels

Fig. 3: TF-domain IS. For OFDM, IS is concentrated along the frequency axis within a time block, while for OTFS, IS is fully spread.

$$\mathbf{P}_{\mathrm{F}}^{I}=\Big|\sum_{p=1}^{P}h_p\Big(\mathbf{F}_M\left(\mathbf{d}_{p,n_0}\odot[\mathbf{F}_M]_{(m_0,:)}^{H}\right)-\frac{1}{M}(\mathbf{1}_M^{T}\mathbf{d}_p)\mathbf{e}_{m_0}\Big)\Big|^{\bullet 2}\mathbf{e}_{n_0}^{T}, \tag{36}$$

$$\mathbf{P}_{\mathrm{T}}^{S}=\frac{1}{MN}\mathbf{1}_M\Big|\sum_{p=1}^{P}h_p\widetilde{\mathbf{d}}_p^{T}\Big|^{\bullet 2}, \tag{37}$$

$$\mathbf{P}_{\mathrm{T}}^{I}=\frac{1}{MN}\mathbf{1}_M\Big|\sum_{p=1}^{P}h_p\left(\widetilde{\mathbf{d}}_{p,m_0}-\widetilde{\mathbf{d}}_p\right)^{T}\Big|^{\bullet 2}. \tag{38}$$

OTFS's SS offers time diversity that increases with $\nu_{\max}$ up to nearly $(P-1)/(2T_{\mathrm{d}})$ and then saturates (see Sec. III-A2). In OFDM, the interference from the i_0th symbol remains confined to the frequency axis within the same (n_0th) time block, whereas in OTFS it spreads over the entire TF domain. Further, the SIR degrades as $\nu_{\max}$ increases for both waveforms.

D. DD-Spread Channels

OTFS simultaneously exploits frequency and time diversity (see Sec. III-A): increasing $\tau_{\max}$ enhances frequency diversity up to nearly $\tau_{\max}=(P-1)/B$, while increasing $\nu_{\max}$ enhances time diversity up to nearly $\nu_{\max}=(P-1)/(2T_{\mathrm{d}})$. Similar to purely Doppler-spread channels, in OFDM, IS remains confined to the frequency axis, whereas OTFS exhibits fully spread TF-domain interference. For both waveforms, the SIR is unaffected by $\tau_{\max}$ but degrades as $\nu_{\max}$ increases. To visualize the SS and IS of OFDM and OTFS, Figs. 2 and 3 present heatmaps of the TF-domain energy for a single symbol at index $i_0=12$ for a system with $M=5$ and $N=5$, which corresponds to the $(2,2)$th TF bin for OFDM and $(2,2)$th DD bin for OTFS. These plots are obtained for one randomly chosen instance of the channel with $P=4$ paths, $\tau_{\max}=2.51$ μs, and $\nu_{\max}=1.85$ kHz. Deep blue indicates low (effectively zero) power, while yellow indicates high power. Fig. 2a illustrates OTFS's SS under purely delay-spread channels, exhibiting row-wise gain variations (frequency diversity); under purely Doppler-spread channels, the pattern rotates by $90°$, yielding column-wise variations (time diversity). Fig. 2b shows OTFS's SS under DD-spread channels, where both time and frequency diversities are present. For OFDM, purely Doppler and DD-spread channels cause interference leakage along the frequency axis within the 2nd time block, as shown in Fig. 3a, while Fig. 3b depicts the IS patterns for OTFS.

E. Duality Between Delay Spread and Doppler Spread

From Sec. IV-B and Sec. IV-C, we observe that delay and Doppler spreads affect the SS and IS structures differently. Delay spread provides frequency diversity without introducing interference and therefore does not degrade the SIR. In contrast, Doppler spread provides time diversity but also introduces interference, degrading SIR as the Doppler spread increases. This asymmetry prevents a direct duality between delay spread and Doppler spread under the considered system model. However, consider an alternative system model in which a DFT is applied along the *time* axis in the TF domain to obtain the frequency-domain signal vector $\mathbf{s}$, followed by CP insertion for each *frequency block* with the CP duration $\Delta f_{\mathsf{CP}} \geq 2\nu_{\max}$. Under a purely Doppler-spread channel, the resulting TF-domain channel matrix becomes diagonal and interference-free. Consequently, the corresponding SS and IS power structures become analogous to those of a purely delay-spread channel. Therefore, the behavior of the considered system model in a purely delay-spread channel can be reproduced by this alternative system model in a purely Doppler-spread channel. In this sense, a purely delay-spread channel under the considered system model may be regarded as the *dual* of a purely Doppler-spread channel under the alternative system model. However, throughout this paper, we adopt the conventional system model of Sec. II, where an IDFT is applied along the *frequency* axis to obtain the time-domain signal vector $\mathbf{s}$, followed by CP insertion for each time block.

So far, we have analyzed the SS and IS of OFDM and OTFS across different channel conditions. In the next section, we examine how these effects, along with the choice of the equalizer, determine the data detection performance.

V. Impact of SS and IS on Equalizer Performance

Recall the characteristics of SS–IS discussed in Sec. III: the SS structure determines the available TF diversity; the IS structure may be concentrated or fully spread over the TF domain; and the associated power levels determine the SIR. The behavior of an equalizer in the presence of these effects can be summarized as follows: *i)* Equalizers benefit from TF diversity induced by the SS structure, and waveforms that offer richer TF diversity generally enable improved data detection performance. *ii)* Interference-agnostic equalizers are strongly affected by the SIR, whereas interference-suppressing or interference-cancelling equalizers are less sensitive to SIR variations. *iii)* Equalizers perform more effectively when the interference exhibits favorable (e.g., concentrated) structures. Based on these observations, we classify equalizers into two broad categories: 1) interference-agnostic equalizers, represented by the 1-tap equalizer, and 2) interference-suppressing equalizers, represented by the FC-MMSE equalizer and the VB-LLR equalizer (discussed in Sec. VI-C). Most practical equalizers can be broadly mapped to one of these two categories and exhibit similar performance.

The received TF-domain signal, $\mathbf{y}_{\mathrm{TF}}$, which we denote by $\mathbf{y}_{\mathrm{F}}$ for OFDM and $\mathbf{y}_{\mathrm{T}}$ for OTFS, is equalized to yield $\widehat{\mathbf{x}}_{\mathrm{TF}}$.[2] From $\widehat{\mathbf{x}}_{\mathrm{TF}}$, the symbol estimates are recovered as follows: (i) for OFDM, $\widehat{\mathbf{x}}_{\mathrm{TF}}$ is directly sliced to obtain $\widehat{\mathbf{x}}$; (ii) for OTFS, $\widehat{\mathbf{x}}_{\mathrm{TF}}$ is first transformed to the DD domain and then sliced to obtain $\widehat{\mathbf{x}}$. The equalization techniques and their performance trends in uncoded communications are discussed below.

A. 1-tap equalizer

This low-complexity ($\mathcal{O}(MN)$) equalizer uses only the diagonal elements of $\mathbf{H}_{\mathrm{TF}}$ and performs symbol-wise detection. Let $\mathbf{H}_{\mathrm{TF}}^{\mathrm{diag}} \triangleq \mathrm{diag}\left(\mathrm{diag}\left(\mathbf{H}_{\mathrm{TF}}\right)\right)$ and $\mathbf{A}_{1-\mathrm{tap}} \triangleq (\mathbf{H}_{\mathrm{TF}}^{\mathrm{diag}^H}\mathbf{H}_{\mathrm{TF}}^{\mathrm{diag}} + \sigma^2\mathbf{I}_{MN})^{-1}\mathbf{H}_{\mathrm{TF}}^{\mathrm{diag}^H}$. The equalization is:

$$\widehat{\mathbf{x}}_{\mathrm{TF}} = \mathbf{A}_{1-\mathrm{tap}}\mathbf{y}_{\mathrm{TF}}. \tag{39}$$

We derive the post-processing SINR to establish the relationship between the SS/IS structures and the BER. In OFDM, the equalized data symbol is $\widehat{\mathbf{x}} = \widehat{\mathbf{x}}_{\mathrm{TF}}$:

$$\widehat{\mathbf{x}} = \mathbf{A}_{1-\mathrm{tap}}(\mathbf{H}_{\mathrm{TF}}^{\mathrm{diag}}\mathbf{x} + \mathbf{H}_{\mathrm{TF}}^{\mathrm{ndiag}}\mathbf{x} + \mathbf{w}_{\mathrm{TF}}), \tag{40}$$

where $\mathbf{H}_{\mathrm{TF}}^{\mathrm{ndiag}} = \mathbf{H}_{\mathrm{TF}} - \mathbf{H}_{\mathrm{TF}}^{\mathrm{diag}}$. The signal component in (40), i.e., $\mathbf{H}_{\mathrm{TF}}^{\mathrm{diag}}\mathbf{x}$, is equivalent to a parallel TF-bin input-output relation. From (16), the SS and IS power vectors for the ith symbol are: $\mathbf{P}_{\mathrm{SS},i} = |\mathbf{H}_{\mathrm{TF}}^{\mathrm{diag}}\mathbf{e}_i|^{\cdot 2}$, and $\mathbf{P}_{\mathrm{IS},i} = |\mathbf{H}_{\mathrm{TF}}^{\mathrm{ndiag}}\mathbf{e}_i|^{\cdot 2}$. Thus, from (40), we can derive the ith symbol's SINR as

$$\mathrm{SINR}_i = P_{\mathrm{SS},i}^{(i)} \Big/ \Big(\sum_{j=0}^{MN-1} P_{\mathrm{IS},j}^{(i)} + \sigma^2\Big), \tag{41}$$

where $P_{\mathrm{SS},i}^{(i)}$ is the ith entry in $\mathbf{P}_{\mathrm{SS},i}$. Assuming BPSK, the error probability of the ith symbol is $P_{e,i} = Q(\sqrt{2\mathrm{SINR}_i})$.

In OTFS, the equalized data symbol is $\widehat{\mathbf{x}} = \mathbf{G}_{\mathrm{T}}^H\widehat{\mathbf{x}}_{\mathrm{TF}}$:

$$\widehat{\mathbf{x}} = \mathbf{G}_{\mathrm{T}}^H\mathbf{A}_{1-\mathrm{tap}}(\mathbf{H}_{\mathrm{TF}}^{\mathrm{diag}}\mathbf{G}_{\mathrm{T}}\mathbf{x} + \mathbf{H}_{\mathrm{TF}}^{\mathrm{ndiag}}\mathbf{G}_{\mathrm{T}}\mathbf{x} + \mathbf{w}_{\mathrm{TF}}). \tag{42}$$

Thus, for the ith entry of $\widehat{\mathbf{x}}$, i.e., $\widehat{x}_i$, the corresponding signal component is given by $\mathbf{G}_{\mathrm{T}}^H\mathbf{H}_{\mathrm{TF}}^{\mathrm{diag}}\mathbf{G}_{\mathrm{T}}\mathbf{e}_i \in \mathbb{C}^{MN}$. We express the associated SS and IS power vectors in the DD domain for the ith symbol as $\mathbf{P}_{\mathrm{SS},i} = |\mathbf{G}_{\mathrm{T}}^H\mathbf{H}_{\mathrm{TF}}^{\mathrm{diag}}\mathbf{G}_{\mathrm{T}}\mathbf{e}_i|^{\cdot 2}$, and $\mathbf{P}_{\mathrm{IS},i} = |\mathbf{G}_{\mathrm{T}}^H\mathbf{H}_{\mathrm{TF}}^{\mathrm{ndiag}}\mathbf{G}_{\mathrm{T}}\mathbf{e}_i|^{\cdot 2}$. Further, the (correct) detection of x_i depends on observations on all MN TF bins (due to $\mathbf{H}_{\mathrm{TF}}^{\mathrm{diag}}\mathbf{G}_{\mathrm{T}}$ term), which are generally correlated since multiple TF bins may experience correlated fading arising from the limited number of propagation paths. Consequently, the number of independent observations available is significantly smaller than MN, making analysis of the effective SINR and BER in DD-spread channels generally intractable. Hence, we present a heuristic analysis below. From Sec. III-A and Sec. III-B, for purely delay- and Doppler-spread channels, the maximum number of independent spectral (effective frequency diversity) and temporal (effective time diversity) components are given by D_{freq} and D_{time}, respectively. For a general DD-spread channel, we define $D_{\mathrm{SS}} = \max(D_{\mathsf{freq}}, D_{\mathsf{time}})$ as the effective

[2] Note that linear equalization can be equivalently carried out in the TF domain or DD domain. In this work, we present the equalization in the TF domain for both OFDM and OTFS. However, symbol slicing and data detection must be performed in the domain where the symbols are mounted.

diversity measure, treating frequency- and time-domain diversity as alternative branches. Let $\mathcal{D}_{\text{SS}}^{(i)}$ denote the corresponding effective TF components for the ith symbol. For each $k \in \mathcal{D}_{\text{SS}}^{(i)}$, we define $\text{SINR}_{i,k} = P_{\text{SS},i}^{(k)}/(\sum_{j\neq i} P_{\text{IS},j}^{(k)} + \sigma^2)$. If we assume that the effective resolvable TF components in $\mathcal{D}_{\text{SS}}$ correspond to D_{SS} independently faded observations corresponding to the ith symbol, for BPSK, we have $P_{e,i} \approx \prod_{k\in\mathcal{D}_{\text{SS}}^{(i)}} Q(\sqrt{2\text{SINR}_{i,k}})$. Defining an equivalent SINR_i such that $Q\left(\sqrt{2\text{SINR}_i}\right) = \prod_{k\in\mathcal{D}_{\text{SS}}^{(i)}} Q\left(\sqrt{2\text{SINR}_{i,k}}\right)$, gives $\text{SINR}_i = (1/2)[Q^{-1}(\prod_{k\in\mathcal{D}_{\text{SS}}^{(i)}} Q(\sqrt{2\text{SINR}_{i,k}}))]^2$. Employing the high-SINR approximation of the Q-function, the equivalent SINR simplifies to $\text{SINR}_i = \sum_{k\in\mathcal{D}_{\text{SS}}^{(i)}} \text{SINR}_{i,k}$. Accordingly, the equivalent SINR for the ith symbol is

$$\text{SINR}_i = \sum\nolimits_{k\in\mathcal{D}_{\text{SS}}^{(i)}} P_{\text{SS},i}^{(k)} \Big/ \Big(\sum\nolimits_{j=0}^{MN-1} P_{\text{IS},j}^{(k)} + \sigma^2\Big), \quad (43)$$

which shows that, in the high-SNR regime, having multiple statistically independent paths can improve the slope of the BER vs. SNR curve.

From the above BER and SINR expressions for OFDM and OTFS, it follows that, for uncoded communications with a 1-tap equalizer, the performance (i) improves with increasing TF diversity (which OFDM cannot exploit), and (ii) degrades as the IS power increases (or equivalently, the SIR decreases), highlighting the interference-agnostic nature of the 1-tap equalizer. Based on these effects, we discuss the behavior of OFDM and OTFS under different channel conditions with the 1-tap equalizer and uncoded transmissions below, where $\approx$ denotes comparable performance.

1) Relative Performance between Waveforms: The relative performance depends solely on TF diversity (since both have the same SIR, see Sec. III-C). The behavior is as follows:

- Flat-fading channels: OFDM $\approx$ OTFS.
- Purely delay-spread channels: OFDM $<$ OTFS.
- Purely Doppler-spread channels: OFDM $<$ OTFS.
- DD-spread channels: OFDM $<$ OTFS.

2) Relative Performance across Channel Conditions: Considering the combined effects of TF diversity and SIR:

- OFDM: No TF diversity in any channel condition; its performance is governed by SIR, yielding DD-spread $\approx$ purely Doppler-spread $<$ purely delay-spread $\approx$ flat-fading. The IS degrades the SIR in purely Doppler-spread channels, leading to poorer performance than in purely delay-spread channels.
- OTFS: In the low-to-moderate SNR regime (practically, $\leq$ 15 dB), the diversity gain dominates over the effect of interference power (equivalently, SIR degradation). The performance ordering becomes flat-fading $<$ purely Doppler-spread/purely delay-spread $<$ DD-spread, since flat-fading channels provide no diversity, purely Doppler-spread channels provide time diversity, purely delay-spread channels provide frequency diversity, and DD-spread channels provide both time and frequency diversity. Between purely Doppler-spread and purely delay-spread channels, the former additionally suffers from interference, whereas the latter does not. Hence, the performance in purely Doppler-spread channels is worse than in purely delay-spread channels. In the high-SNR regime, however, the effect of interference dominates over that of additive noise. Hence, the BER is primarily governed by the interference power. As a result, purely Doppler-spread/DD-spread $<$ flat-fading/purely delay-spread. Within these groups, the diversity gain determines the relative ordering: purely Doppler-spread $<$ DD-spread because DD-spread channels additionally provide frequency diversity compared to purely Doppler-spread channels, and flat-fading $<$ purely delay-spread again because purely delay-spread channels additionally provide frequency diversity compared to flat-fading channels. In summary, the ordering is (i) Low/moderate-SNR regime: flat-fading $<$ purely Doppler-spread $<$ purely delay-spread $<$ DD-spread, (ii) High SNR regime: purely Doppler-spread $<$ DD-spread $<$ flat-fading $<$ purely delay-spread. Thus, crossover occurs between flat-fading and purely Doppler-spread channels, and between purely delay-spread and DD-spread channels.

3) Effect of Increasing $\tau_{\max}$: From Sec. III, increasing $\tau_{\max}$ enhances the frequency diversity of OTFS until $\tau_{\max}$ reaches at least $(P-1)/B$, while having no impact on SIR.

- OFDM: Performance remains unchanged with $\tau_{\max}$.
- OTFS: Performance improves with increasing $\tau_{\max}$ up to nearly $\tau_{\max} = (P-1)/B$, beyond which it approaches saturation as the maximum frequency diversity is reached.

4) Increasing $\nu_{\max}$: Increasing $\nu_{\max}$ increases the time diversity of OTFS up to nearly $\nu_{\max} = (P-1)/(2T_{\text{d}})$, while the SIR monotonically degrades with SIR for both waveforms. This creates a diversity–SIR tradeoff for OTFS.

- OFDM: Performance degrades monotonically with $\nu_{\max}$.
- OTFS: Performance initially improves due to time diversity and then drops because SIR deterioration dominates. Although the time diversity saturates at nearly $\nu_{\max} = (P-1)/2T_{\text{d}}$, performance may start worsening earlier due to the monotonic SIR degradation.

B. Full-complexity MMSE (FC-MMSE) equalizer

The FC-MMSE equalizer exploits the full channel matrix:

$$\widehat{\mathbf{x}}_{\text{TF}} = \left(\mathbf{H}_{\text{TF}}^H \mathbf{H}_{\text{TF}} + \sigma^2 \mathbf{I}_{MN}\right)^{-1} \mathbf{H}_{\text{TF}}^H \mathbf{y}_{\text{TF}}. \quad (44)$$

Its computational complexity is $\mathcal{O}(M^3N^3)$, significantly higher than the 1-tap equalizer. Unlike the 1-tap equalizer, FC-MMSE suppresses interference through matrix inversion. Therefore, its performance mainly depends on the higher TF diversity, which improves performance. It is largely insensitive to SIR. The presence of IS leads to a non-diagonal channel matrix ($\mathbf{H}_{\text{TF}}$), but the FC-MMSE equalizer can coherently combine multiple Doppler-shifted components of each symbol through the term $\mathbf{H}_{\text{TF}}^H \mathbf{H}_{\text{TF}}$. Consequently, the post-equalization SINR derived from (44) contains additional signal-power terms contributed by the off-diagonal channel entries, leading to an increase in the effective SINR. We refer to this as the *equalizer gain*. Although this effect is relatively weak compared to diversity gain induced by the SS structure, it nevertheless provides an additional performance improvement and is empirically illustrated in Sec. VII-A.

1) Relative Performance across Waveforms: Based on the TF diversity, the relative performance is:

- Flat-fading channels: OFDM $\approx$ OTFS

- Purely delay-spread channels: OFDM $<$ OTFS.
- Purely Doppler-spread channels: OFDM $<$ OTFS.
- DD-spread channels: OFDM $<$ OTFS.

2) Relative Performance across Channels: Considering both TF diversity and equalizer gain:

- OFDM: Equalizer gain governs performance: Flat-fading $\approx$ purely delay-spread $<$ purely Doppler-spread $\approx$ DD-spread.
- OTFS: Flat-fading $<$ purely delay-spread $<$ purely Doppler-spread $<$ DD-spread.

3) Increasing $\tau_{\max}$: From Sec. III, increasing $\tau_{\max}$ enhances the frequency diversity of OTFS up to nearly $\tau_{\max} = (P-1)/B$, while having no impact on equalizer gain.

- OFDM: Performance is unchanged with increasing $\tau_{\max}$.
- OTFS: Performance improves with $\tau_{\max}$ up to nearly $\tau_{\max} = (P-1)/B$, beyond which it approaches saturation.

4) Increasing $\nu_{\max}$: Increasing $\nu_{\max}$ enhances the time diversity of OTFS up to nearly $\nu_{\max} = (P-1)/(2T_{\mathrm{d}})$ and gradually increases the equalizer gain for both waveforms.

- OFDM: Performance improves slowly with increasing $\nu_{\max}$ due to equalizer gain.
- OTFS: Performance improves monotonically with $\nu_{\max}$ up to nearly $\nu_{\max} = (P-1)/(2T_{\mathrm{d}})$ and then improves marginally (equalizer gain), appearing nearly saturated. Since FC-MMSE is insensitive to SIR, the diversity–SIR tradeoff observed with the 1-tap equalizer does not arise in this case.

Note that, in the above uncoded scenarios, the relative performance of OFDM and OTFS under different channel conditions is governed solely by TF diversity: OTFS inherently exploits TF diversity, whereas OFDM does not. Consequently, although OFDM exhibits a more concentrated IS structure (see Sec. III-B) than OTFS, it does not translate into any gains in uncoded transmissions. The IS-structure-advantage of OFDM becomes pronounced only when OFDM attains TF diversity comparable to OTFS, e.g., via channel coding. Then, the *IS structure* governs performance, allowing *OFDM to potentially outperform OTFS*. In the next section, we examine the origin of TF diversity in uncoded OTFS, and then investigate how a similar TF diversity can be achieved with OFDM.

VI. Spreading with Coded Communications

A. Source of TF diversity in OTFS

Focusing on DD-spread channels, the main reason for the performance advantage of OTFS over OFDM lies in the SS-induced TF diversity introduced by the ISFFT-based preprocessing. The TF-domain channel $\mathbf{H}_{\mathrm{TF}}$ exhibits different gains across TF bins (determined by $\boldsymbol{\gamma}_p$ and $\widetilde{\mathbf{d}}_p$). In OFDM, each symbol occupies a single TF bin and therefore experiences only the corresponding channel gain. In contrast, the ISFFT in (2) spreads each DD-domain symbol across all TF bins, allowing it to experience all TF-domain channel gains and thereby achieve TF diversity. To better understand the role of this spreading, we consider a weighted ISFFT that restricts TF-domain spreading and study how this impacts TF-domain diversity. Specifically, we define a weighted ISFFT operation:

$$X[n,m] = \frac{1}{\sqrt{NM}} \sum_{k=0}^{N-1} \sum_{l=0}^{M-1} w_\tau(k,n) x[k,l] w_\nu(l,m) \times e^{j2\pi\left(\frac{nk}{N} - \frac{ml}{M}\right)},$$

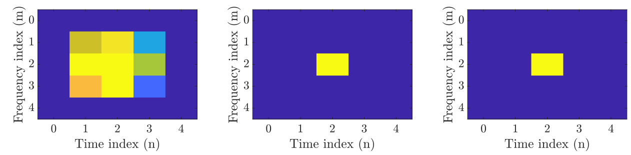

(a) OTFS for $\alpha = 0.4$ **(b)** OTFS for $\alpha = 1$ **(c)** OFDM

Fig. 4: TF-domain SS of OTFS for different α and OFDM. As α transitions from 0 to 1, the SS of OTFS becomes similar to that of OFDM.

where the delay-domain and Doppler-domain weights are given by $w_\tau(k,m) = e^{-\alpha(k-m)^2}$ and $w_\nu(l,n) = e^{-\alpha(l-n)^2}$, respectively, and α controls how much spreading occurs. The above weighted ISFFT serves as a structural analysis tool to isolate the role of spreading in governing SS and IS behavior: when $\alpha = 0$, the weighted ISFFT reduces to the conventional ISFFT, yielding fully spread OTFS symbols (see Fig. 2b.) As α increases, TF-domain spreading progressively reduces. For the 5×5 OTFS system considered here for illustration, TF diversity largely vanishes around $\alpha = 1$, at which point the SS behavior becomes comparable to that of OFDM. This effect is illustrated in Fig. 4. Thus, OTFS and OFDM can be viewed as operating points on a broader spreading-localization continuum. As spreading increases, TF diversity improves through the SS structure, while interference becomes more widely distributed through the IS structure. This is also why OTFS benefits from interference-aware qualizers.

In uncoded transmissions, this ISFFT-induced TF diversity is unavailable in OFDM. This motivates the use of channel coding to induce TF-domain spreading in OFDM, since coding couples symbols mounted on different TF bins. In the next subsection, we analyze LDPC-coded OFDM and OTFS and study the resulting TF diversity in both waveforms. In this work, we consider the LDPC code due to its widespread use in modern standards, but the insights readily extend to other coding schemes also.

B. Spreading in LDPC-Coded Systems

We consider an LDPC-coded communication system with the same system parameters M, N, Δf, and T_{d} as described in Sec. II, for both OFDM and OTFS. At the transmitter, the data bits $\mathbf{u} \in \{0,1\}^I$ are encoded using an LDPC code of rate $R = I/I'$. The resulting coded bits $\mathbf{u}' \in \{0,1\}^{I'}$ are mapped to a $Q-$QAM constellation, yielding $\mathbf{x} \in \mathbb{C}^{MN}$, where $MN = I'/\log_2(Q)$. The symbols are arranged in an $M \times N$ 2D grid and mapped onto the TF domain (for OFDM) or DD domain (for OTFS). The corresponding received signal vector is used to compute the LLRs of the coded bits $\mathbf{u}'$, which are then fed to the LDPC decoder to obtain the estimated data bits $\hat{\mathbf{u}}$.

The LDPC code can be defined by a generator matrix $\mathbf{G}_{\mathrm{LDPC}} \in \{0,1\}^{I' \times I}$, from which the encoded bits are obtained as $\mathbf{u}' = \mathbf{G}_{\mathrm{LDPC}}\mathbf{u} \mod 2$. To analyze the SS in coded communication, we set i_0th bit of $\mathbf{u}$ to 1 and all others to zero, then the encoded bits become $\mathbf{G}_{\mathrm{LDPC}}\mathbf{e}_{i_0}$. The corresponding symbol vector becomes $\mathbf{x}_{i_0} = f_{\mathrm{mod}}(\mathbf{G}_{\mathrm{LDPC}}\mathbf{e}_{i_0})$ after constellation mapping, where $f_{\mathrm{mod}}(\cdot)$ denotes bits to $Q-$QAM

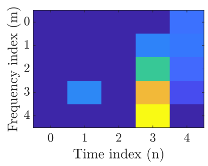

(a) LDPC code rate$=16/25$

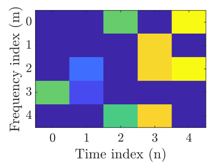

(b) LDPC code rate$=6/25$

Fig. 5: TF-domain SS for OFDM with coded communication. As the code rate reduces, there is more symbol spreading, leading to higher TF-diversity.

symbol mapping and let $\Delta\mathbf{x}_{i_0} = f_{\text{mod}}(\mathbf{G}_{\text{LDPC}}\mathbf{e}_{i_0}) - f_{\text{mod}}(\mathbf{0})$. Then, for OFDM and OTFS, the SS is given by

$$\mathbf{P}_{\text{F}}^{S} = \text{vec}^{-1}(|\text{diag}(\mathbf{H}_{\text{TF}}) \odot \Delta\mathbf{x}_{i_0}|^{\cdot 2}), \quad (45)$$

$$\mathbf{P}_{\text{T}}^{S} = \text{vec}^{-1}(|\text{diag}(\mathbf{H}_{\text{TF}}) \odot [\mathbf{G}_{\text{T}}\Delta\mathbf{x}_{i_0}]|^{\cdot 2}). \quad (46)$$

In OTFS, the ISFFT preprocessing $\mathbf{G}_{\text{T}}$ already induces full TF-domain spreading even in uncoded transmission. Therefore, we focus on OFDM to understand how channel coding enables TF-domain spreading and diversity. From (45), OFDM's SS is now governed by the LDPC structure $\mathbf{G}_{\text{LDPC}}$, unlike the uncoded case, where the symbol energy is confined to a single TF bin. Fig. 5 illustrates the TF-domain SS of 5×5 OFDM for two LDPC code rates, evaluated at symbol index $i_0 = \lfloor I/2 \rfloor$, in DD-spread channels. As the code rate decreases from $16/25$ to $6/25$, the spreading becomes more pronounced, leading to increased TF diversity. This demonstrates that channel coding enables OFDM to extract TF diversity, with lower code rates providing stronger spreading and hence higher diversity. For OTFS, since full TF diversity is already present without coding, the additional gain from coding primarily arises from coding gain (also available to OFDM), determined by the Euclidean distance between codewords [9], [21]. As a result, at sufficiently low code rates, OFDM can achieve performance comparable to OTFS.

In Sec. V, we analyzed the 1-tap and FC-MMSE equalizers for uncoded systems. In coded systems, their soft outputs can be fed to the LDPC decoder to identify the code rates at which OFDM approaches OTFS. However, both equalizers require very low code rates, as they are not designed for reliable LLR generation. This motivates advanced soft-detection algorithms that produce reliable LLRs for LDPC decoding.

C. Variational Bayesian-Based LLR Generation

We now present a novel low-complexity variational Bayesian-based LLR (VB-LLR) algorithm for computing reliable LLRs to be input to the LDPC decoder. The idea is to approximate the marginal posterior distribution of data symbols $\mathbf{x}$, and use it to compute the LLRs. Let $\mathbf{H} = \mathbf{H}_{\text{TF}}$, $\mathbf{y} = \mathbf{y}_{\text{TF}}$ for OFDM and $\mathbf{H} = \mathbf{H}_{\text{DD}}$, $\mathbf{y} = \mathbf{y}_{\text{DD}}$ for OTFS. We assume that the prior on the data symbols is i.i.d. and uniform over the $Q-$QAM constellation, i.e., $\text{P}_{x_i}(z) = 1/Q, \forall z \in \mathbb{Q}$. The VB technique iteratively updates the marginals $\{q_i(x_i)\}$. At the $(j+1)$th iteration, the update for $q_i(x_i)$ is obtained by

$$\ln q_i^{(j+1)}(z) \propto \langle \ln p(\mathbf{y}|\mathbf{H}, \mathbf{x}) + \ln \text{P}_{x_i}(z) \rangle_{\{q_k^{(j)}(x_k)\}_{k\neq i}}$$

$$\propto -\frac{1}{\sigma_{\text{d}}^2}\|\mathbf{y} - [\mathbf{H}]_{(:,i)}z - [\mathbf{H}]_{(:,\neq i)}\langle \mathbf{x}\rangle_{\neq i}^{(j)}\|^2 \triangleq f_i^{(j+1)}(z), \quad (47)$$

TABLE II: Complexity comparison of considered equalizers

Receiver	Computational Complexity
1-tap Equalizer	$\mathcal{O}(MN)$
FC-MMSE	$\mathcal{O}((MN)^3)$
MP Detector	$\mathcal{O}(I_{\text{MP}}MN(MN + N_I + Q))$
VB-LLR (Proposed)	$\mathcal{O}(I_{\text{VB}}M^2N^2)$

where $\langle x_i \rangle^{(j)} = \sum_{z\in\mathbb{Q}} z q_i^{(j)}(z)$ and $\langle \mathbf{x}\rangle^{(j)} = [\langle x_0\rangle^{(j)}, \ldots, \langle x_{MN-1}\rangle^{(j)}]^T \in \mathbb{C}^{MN}$. The expression in (47) leads to the normalized update $q_i^{(j+1)}(z) = e^{f_i^{(j+1)}(z)} / \sum_{z'\in\mathbb{Q}} e^{f_i^{(j+1)}(z')}$. The above iterative procedure follows the minorization-maximization (MM) principle and converges to a stationary point of the evidence lower bound from any initialization [26]. Upon convergence, the LLRs of the coded bits $\mathbf{u}'$ associated with the symbols in $\mathbf{x}$ are computed from the marginals. For each bit position $b \in \{0, \ldots, \log_2 Q - 1\}$ of symbol x_i, the LLR is given by $\Lambda_{i,b} = \ln(\sum_{z\in\mathcal{Z}_{b=0}} q_i(z) / \sum_{z\in\mathcal{Z}_{b=1}} q_i(z))$, where $\mathcal{Z}_{b=k}$ is the subset of constellation points from $\mathbb{Q}$ whose bth bit is k, where $k \in \{0, 1\}$. Since VB-LLR is specifically designed for LLR generation, it produces higher-quality soft information than the 1-tap and FC-MMSE equalizers, allowing similar performance to be achieved at higher code rates, as demonstrated in Sec. VII.

Message passing (MP) [7] is an algorithm similar to VB-LLR for soft symbol detection and LLR generation. MP approximates the interference associated with x_i as a complex Gaussian random variable whose mean and variance are computed from the current beliefs and iteratively updates symbol marginals. If the variance of the interference is fixed to a constant value, σ^2, the MP update reduces to (47), which corresponds to the VB-LLR update. Thus, VB-LLR can be interpreted as a simplified version of MP where only the mean of the interference is used. The main advantages of VB-LLR are: being based on the MM principle, it is guaranteed to converge from any initialization; it eliminates the need to compute interference variance and therefore incurs lower per-iteration computational cost than MP while retaining a structurally similar update mechanism. The required number of iterations can depend on the system parameters and channel conditions Additionally, while VB-LLR employs a factorized approximation of the posterior distribution, MP does not; instead, it approximates the interference as following a Gaussian distribution. We present a consolidated complexity comparison of the 1-tap, FC-MMSE, MP, and proposed VB-LLR detectors in Table II, where N_I denotes the number of effective interference interactions induced by the IS structure, and I_{MP} and I_{VB} denote the numbers of MP and VB-LLR iterations, respectively. Although VB-LLR has lower per-iteration complexity than MP, I_{MP} and I_{VB} may vary with the system parameters and channel conditions; hence, the lower per-iteration complexity does not necessarily imply lower total complexity. In our simulations, however, the two algorithms require similar numbers of iterations, while VB-LLR achieves the same BER performance as MP, in the considered scenarios. As discussed in Sec. V, although

TABLE III: System parameters for OFDM and OTFS

M	N	Δf	$T = \frac{1}{\Delta f}$	f_c
32	8	15 kHz	66.6 μs	4 GHz

TABLE IV: Parameters for DD-spread channels

P	$\tau_{\max}$	$v_{\max}$ (max. speed)	$\nu_{\max} = \frac{v_{\max}}{c} f_c$
4	2.51 μs	500 kmph	1.85 kHz

OFDM has a more concentrated IS structure than OTFS, this advantage is masked in uncoded transmission by the TF diversity of OTFS. When the code rate is sufficiently low, coding enables OFDM to attain TF diversity comparable to OTFS. At that point, OFDM's concentrated IS structure becomes beneficial, allowing the equalizer to produce higher-quality soft information than OTFS with its fully spread IS. Consequently, OFDM can outperform OTFS at low code rates, as shown in Sec. VII-B.

VII. Simulation Results

In this section, we evaluate the performance of OFDM and OTFS across different channel conditions and equalizers, and corroborate our theoretical insights. We consider data transmission with system parameters as in Table III [27], [28]. The channel is DD-spread, with parameters as in Table IV [27]. We generate the channel parameters as: $h_p \overset{i.i.d.}{\sim} \mathcal{CN}(0, 1/P)$, $\tau_p \overset{i.i.d.}{\sim} \mathcal{U}(0, \tau_{\max})$, and $\nu_p \overset{i.i.d.}{\sim} \mathcal{U}(-\nu_{\max}, \nu_{\max})$ [29]. The CP duration $T_{\mathsf{CP}} = \tau_{\max}$, bandwidth $B = 0.48$ MHz, and total time-duration $T_{\mathrm{d}} = 0.55$ ms. The data symbols are drawn uniformly at random from the BPSK constellation, except for Fig. 11b, where they are drawn from a 16-QAM constellation. We assume perfect channel-state information at the receiver (CSIR). We have verified that the observed performance trends remain unchanged when practical high-quality channel estimation schemes, such as [16], are employed (see Fig. 11a). We present results for uncoded and LDPC-coded OFDM and OTFS transmissions.

A. Uncoded Data Detection Results

We evaluate the data detection performance of OFDM and OTFS in uncoded communications under various channel conditions using different equalizers and demonstrate that the trends are consistent with the analytical insights from Sec. V.

1) Uncoded BER vs. SNR with 1-tap equalizer (Fig. 6a): *i)* In flat-fading channels, OFDM $\approx$ OTFS. In all other channels, OTFS consistently outperforms OFDM due to its TF diversity (see Sec. V-A1). Specifically, in purely delay-spread channels, at BER $= 10^{-2}$, OTFS achieves 3.2 dB improvement over OFDM. *ii)* Both OFDM and OTFS exhibit BER floors in purely Doppler-spread and DD-spread channels (beyond $\approx$ 18 dB SNR) due to the IS power level (see Sec. V-A2). For OFDM, purely Doppler-spread and DD-spread channels show comparable BER owing to their similar SS/IS effects. Similarly, flat-fading and purely delay-spread channels also yield identical BER. Moreover, the latter pair outperforms the former by about 1.8 dB at BER $= 10^{-2}$, due to the absence of IS. For OTFS, purely delay-spread channels outperform flat-fading channels by about 3.1 dB at BER $= 10^{-2}$ due to the additional frequency diversity, with both cases exhibiting zero IS power and monotonically decreasing BER. In contrast, SIR degradation (due to IS power) causes purely Doppler and DD-spread channels to exhibit BER floors at 1.2×10^{-3} and 4.8×10^{-4}. Up to an SNR of $\sim$ 22 dB, purely Doppler-spread channels outperform flat-fading owing to time diversity; beyond this point, IS power dominates, leading to a crossover. A similar crossover occurs between purely delay-spread and DD-spread channels, at an SNR of ≈ 18 dB.

2) Uncoded BER vs. SNR with FC-MMSE equalizer (Fig. 6b): *i)* In flat-fading channels, OFDM and OTFS exhibit comparable performance, whereas OTFS outperforms OFDM in all other channel conditions due to TF diversity (see Sec. V-B1)–e.g., by about 3.8 dB at BER $= 10^{-2}$ in DD-spread channels. *ii)* Since FC-MMSE suppresses interference, with OFDM, purely Doppler-spread $\approx$ DD-spread channels and purely delay-spread $\approx$ flat-fading channels, and the former pair outperforms the latter by approximately 2.5 dB at BER $= 10^{-3}$ due to equalizer gain. For OTFS, the best performance is seen in DD-spread channels, followed by purely Doppler-spread, purely delay-spread, and flat-fading channels, due to both TF diversity and equalizer gain (see Sec. V-B2). For instance, at BER $= 10^{-3}$, purely Doppler-spread channels outperform purely delay-spread channels by 1 dB (due to equalizer gain), while purely delay-spread channels outperform flat-fading channels by 6.3 dB (due to frequency diversity).

3) Uncoded BER vs. SNR with the VB-LLR equalizer (Fig. 6c): Although the VB-LLR decoder (see Sec. VI-C) is designed for coded communication, it can also be applied to the uncoded case by slicing the soft symbol outputs. The VB-LLR acts as an interference-canceling detector and follows trends similar to FC-MMSE. Notably, it outperforms both 1-tap and FC-MMSE equalizers, especially in DD-spread channels, due to its nonlinear iterative posterior computation. For example, under DD-spread channels, with OTFS, VB-LLR provides a 2 dB gain over FC-MMSE at BER $= 10^{-3}$.

4) Uncoded BER vs. $\tau_{\max}$ (Fig. 7a): We vary $\tau_{\max}$ from 0 to 7 μs, keeping other channel parameters fixed (as per Table IV), with $T_{\mathsf{CP}} = \tau_{\max}$. At $\tau_{\max} = 0$, the channel is a purely Doppler-spread, and the performance trends match earlier observations. The main observations, in line with Secs. V-A3 and V-B3, are as follows: *i)* OTFS outperforms OFDM for all $\tau_{\max}$. It exploits time diversity at $\tau_{\max} = 0$ and gains additional frequency diversity as $\tau_{\max}$ increases up to nearly $\tau_{\max} = (P-1)/B = 6.25$ μs, leading to BER improvement until this point and saturation thereafter. *ii)* OFDM exhibits an error floor for all equalizers (e.g., around 6×10^{-3} under FC-MMSE), since $\tau_{\max}$ does not impact SIR.

5) Uncoded BER vs. $\nu_{\max}$ (Fig. 7b): We vary $\nu_{\max}$ from 0 to 4 kHz. At $\nu_{\max} = 0$, the channel reduces to a purely delay-spread channel, and the performance trends are consistent with earlier results. The key observations (see Secs. V-A4 and V-B4) are: *i)* OTFS outperforms OFDM for all $\nu_{\max}$, exploiting frequency diversity at $\nu_{\max} = 0$ and additional time diversity as $\nu_{\max}$ increases. *ii)* With the 1-tap equalizer, OFDM exhibits a monotonic BER degradation with increasing $\nu_{\max}$

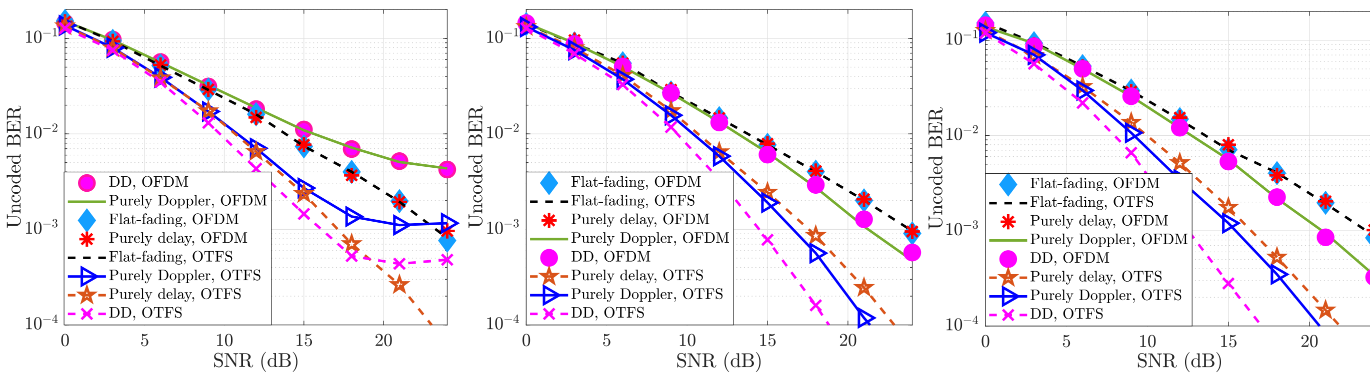

(a) 1-tap equalizer. **(b)** FC-MMSE equalizer. **(c)** VB-LLR equalizer.

Fig. 6: Uncoded BER vs. SNR under different equalizers and channel conditions ($M = 32$, $N = 8$, $P = 4$): (a) TF diversity and SIR degradation govern the performance, whereas (b) and (c) TF diversity and equalizer gain govern the performance. OTFS generally outperforms OFDM, especially in DD-spread channels, with both benefiting from more sophisticated (FC-MMSE, VB-LLR) equalizers.

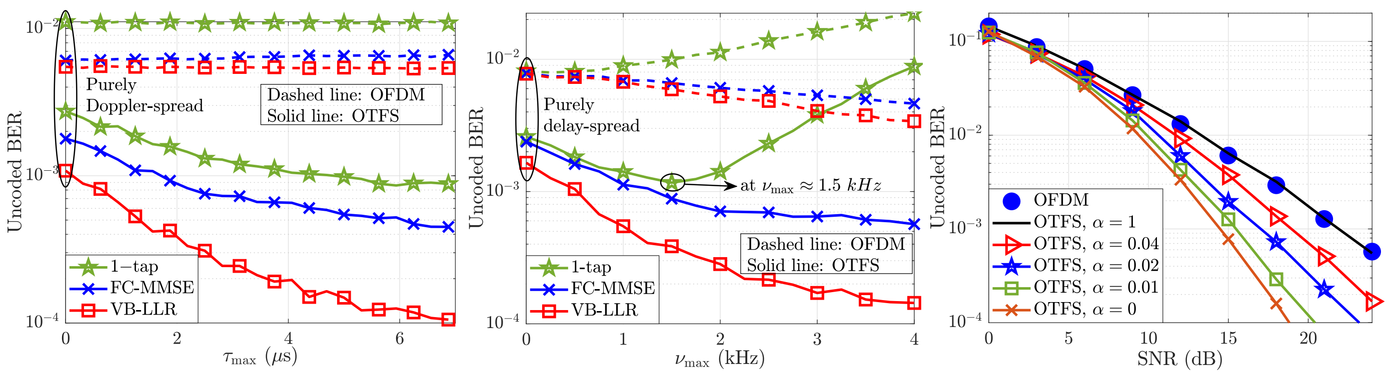

(a) Uncoded BER vs. $\tau_{\max}$ under different equalizers. **(b)** Uncoded BER vs. $\nu_{\max}$, under different equalizers. **(c)** Uncoded BER vs. SNR with different α.

Fig. 7: Uncoded performance in DD-spread channels: (a) impact of $\tau_{\max}$ at $\nu_{\max} = 1.85$ kHz, SNR $= 15$ dB, illustrating frequency diversity; (b) impact of $\nu_{\max}$ at $\tau_{\max} = 2.51$ μs, SNR $= 15$ dB, illustrating the time-diversity/SIR tradeoff. OTFS extracts both time and frequency diversity, yielding improved performance with increasing $\tau_{\max}$ and $\nu_{\max}$ under FC-MMSE and VB-LLR, whereas with a 1-tap equalizer, its performance improves with $\nu_{\max}$ up to a point, beyond which increased interference causes degradation; (c) impact of α on OTFS with FC-MMSE, showing its transition toward OFDM as α increases.

due to SIR deterioration. In contrast, OTFS initially benefits from inceasing time diversity, leading to BER improvement, but after $\nu_{\max} \approx 1.5$ kHz, the BER starts to degrade as SIR degradation dominates. *iii)* With interference-suppressing equalizers (FC-MMSE, VB-LLR), OFDM shows a slow BER improvement with $\nu_{\max}$ due to equalizer gain. For OTFS, the BER improves monotonically up to 2.7 kHz (where full time diversity is achieved), beyond which the improvement becomes marginal. That is, beyond 2.7 kHz, the OFDM and OTFS curves for the same equalizer become parallel, despite an order-of-magnitude performance gap.

6) Uncoded BER vs. SNR for different α (Fig. 7c): In DD-spread channels, $\alpha = 0$ corresponds to OTFS with full TF SS. As α increases from 0.01 to 0.04, SS progressively decreases, reducing TF diversity and, consequently, degrading BER. For large α (e.g., $\alpha = 1$), the SS vanishes, and OTFS exhibits the same symbol localization as OFDM, resulting in identical performance. *This confirms that the performance advantage of OTFS over OFDM in uncoded communications arises solely from ISFFT-induced SS and the associated TF diversity.*

B. Coded Data Detection Results

We evaluate the relative performance of OFDM and OTFS over DD-spread channels under LDPC-coded transmissions. We feed three different qualities of soft symbols, generated by 1-tap, FC-MMSE, and the proposed VB-LLR equalizer, to the LDPC decoder. We also select the LDPC code rates R from the 5G-NR MCS table in [30] and use the common system and channel parameters listed in Table III and IV for all simulations. As a baseline observation, for all equalizers and code rates, the coded BER (Fig. 8a- 8c) outperforms their uncoded counterparts. The key observations are:

1) Coded BER vs. SNR (Fig. 8a- 8c): For each equalizer, we consider three code rates corresponding to high, moderate, and low values. *i) 1-tap soft symbols (Fig. 8a):* At $R = 0.554$, OTFS outperforms OFDM by approximately 3 dB at BER $= 10^{-2}$. Although channel coding enables OFDM to benefit from TF diversity, the diversity achieved at this rate remains lower than that offered by SS in OTFS. At $R = 0.245$, the TF diversity of OFDM improves further, resulting in performance comparable to OTFS. When the code rate is reduced to $R = 0.117$, *OFDM outperforms OTFS*: for example, at BER $= 10^{-5}$, OFDM achieves a gain of about 0.9 dB. At this low rate, both waveforms achieve similar TF diversity, and the relative performance is primarily governed by IS structure. The fact that the IS is concentrated along the frequency axis in OFDM allows for better interference cancelation (see Sec. III-B), resulting in higher quality soft

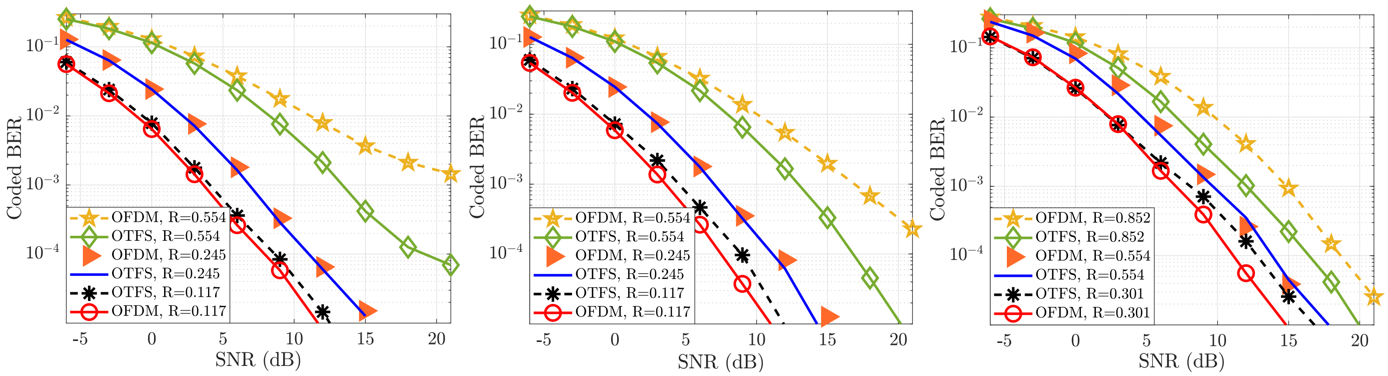

(a) 1-tap soft-symbols. **(b)** FC-MMSE soft symbols. **(c)** VB-LLR soft-symbols.

Fig. 8: Coded BER vs. SNR in DD channels with different equalizers and code rates ($\tau_{\max} = 2.51$ μs, $\nu_{\max} = 1.85$ kHz), illustrating SS/IS structures. OFDM matches OTFS at $R = 0.245$ (1-tap/FC-MMSE) and $R = 0.554$ (VB-LLRs), and outperforms it at $R = 0.117$ and $R = 0.301$, respectively. Thus, with coding, the performance differences between OFDM and OTFS are greatly diminished.

symbols than in OTFS and leading to improved performance. *ii) FC-MMSE soft symbols:* The FC-MMSE equalizer produces higher-quality soft symbols than the 1-tap equalizer, so the BER (Fig. 8b) no longer exhibits early error floors, particularly at $R = 0.554$. Similar to the 1-tap case, OFDM and OTFS exhibit comparable performance at $R = 0.245$. At $R = 0.117$, OFDM again outperforms OTFS. Specifically, at BER $= 10^{-5}$, OFDM outperforms OTFS by 1 dB. *iii) VB-LLRs:* The VB-LLR equalizer is explicitly designed to generate high-quality LLRs, and therefore achieves the best overall performance (Fig. 8c). For instance, at a high code rate $R = 0.852$, OFDM reaches BER $= 10^{-3}$ at SNR ≈ 15 dB, which is nearly 2 dB better than the FC-MMSE equalizer operating at a lower rate ($R = 0.554$). Also, even at $R = 0.852$, the gap between OFDM and OTFS is relatively small compared to that observed with the 1-tap and FC-MMSE equalizers. At lower code rates, similar trends to the FC-MMSE case are observed. In particular, at $R = 0.554$, OFDM performs on par with OTFS and at $R = 0.301$, OFDM outperforms OTFS by about 2 dB at BER $= 10^{-5}$. This is due to the interference-cancellation capability of the VB-LLR equalizer, which is more effective in OFDM owing to its more concentrated IS structure than in OTFS.

2) Coded BER vs. $\tau_{\max}$ and $\nu_{\max}$ (Figs. 9 and 10): We consider the low complexity 1-tap equalizer (Fig. 9) and the interference-cancelling VB-LLR equalizer (Fig. 10). *i)* Under both equalizers, increasing $\tau_{\max}$ improves OFDM and OTFS performance, unlike in the uncoded case. This is due to the frequency diversity enabled by channel coding, and is more pronounced at lower code rates and high-quality soft symbols (VB-LLR). *ii)* With 1-tap soft symbols, increasing $\nu_{\max}$ initially reduces the BER for both waveforms due to higher time diversity, but beyond a certain point, the BER marginally increases as SIR degradation dominates. *iii)* With the VB-LLR equalizer, the BER decreases monotonically with increasing $\nu_{\max}$, as SIR has a negligible impact. *iv)* With both equalizers, OFDM outperforms OTFS at low code rates (e.g., $R = 0.117$ for 1-tap and $R = 0.301$ for VB-LLR) for all $\tau_{\max}$ and $\nu_{\max}$, with a more pronounced gap under VB-LLR. Coding enables OFDM to achieve TF diversity comparable to OTFS *and* benefit from its concentrated IS structure, whereas

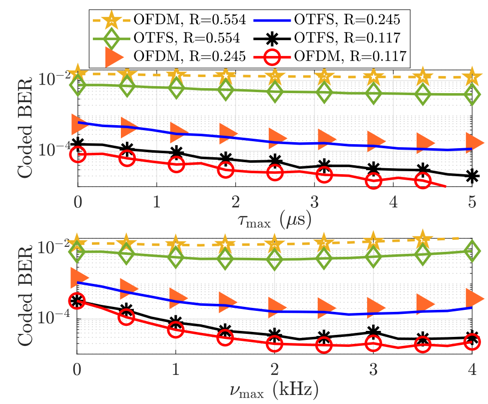

Fig. 9: Coded BER vs. $\tau_{\max}$, $\nu_{\max}$ with 1-tap soft-symbols at SNR= 10 dB.

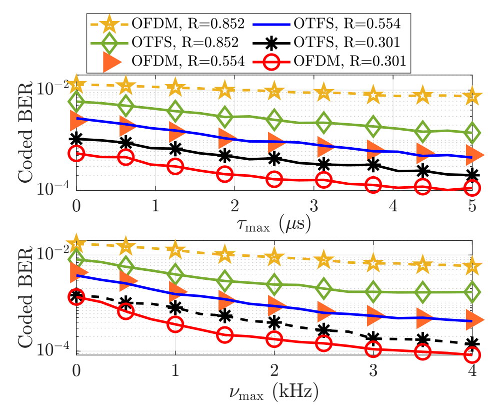

Fig. 10: Coded BER vs. $\tau_{\max}$ and $\nu_{\max}$ with VB-LLRs at SNR= 10 dB.

OTFS suffers from fully spread IS. At $\nu_{\max} = 0$ (purely delay-spread), both waveforms exhibit the same performance due to zero IS. Finally, except for the 1-tap case, with varying $\nu_{\max}$ (where SIR plays a role), the gap between OFDM and OTFS is nearly constant, since neither of them alter the IS structure (see Sec. III-B). This shows that OFDM's advantage at low code rates arises from its concentrated IS structure.

C. Uncoded BER with estimated channel

We present the BER using the second-order variational Bayesian off-grid channel estimation algorithm of [16]

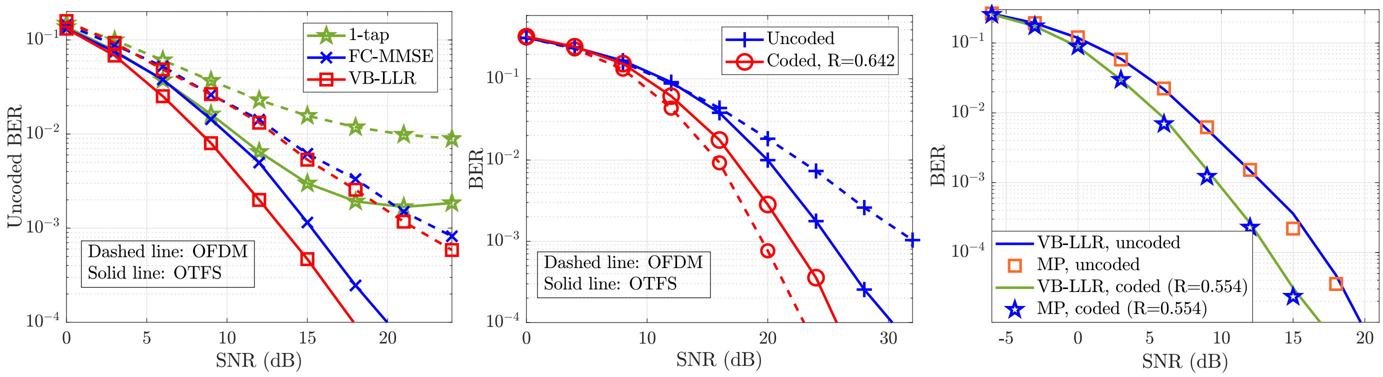

(a) Estimated channel. **(b)** 16-QAM with VB-LLR. **(c)** Comparison of the VB-LLR and MP for OTFS.

Fig. 11: BER vs. SNR: (a) channel-estimation trends remain consistent with perfect CSI; (b) higher-order constellations make the receivers more sensitive to interference; (c) both detectors achieve the same performance.

in Fig. 11a. We use a 32-symbol preamble as a pilot signal for channel estimation, with the pilot signal mounted on an 8×4 DD/TF grid for OTFS/OFDM, respectively. The pilot SNR is set to be equal to the data SNR; all other settings are the same as in Fig. 6. Compared with the perfect-CSIR results in Fig. 6, the BER degradation due to channel estimation is relatively small. For example, under FC-MMSE equalization, the loss at a BER of 10^{-3} is approximately 0.8 dB. The 1-tap equalizer experiences a larger degradation because it relies solely on the diagonal entries of the effective channel matrix and is therefore more sensitive to channel estimation errors. However, the overall performance trends remain unchanged. In particular, the BER improvement, saturation behavior, and crossover characteristics observed under perfect CSIR are preserved under estimated CSIR.

D. BER with 16-QAM Constellation

Fig. 11b presents the BER of OFDM and OTFS employing the VB-LLR equalizer with a 16-QAM constellation. In the uncoded case, the performance gap between OFDM and OTFS is smaller than in the BPSK case. For example, at a BER of 10^{-2}, OTFS provides about 2.5 dB gain over OFDM, whereas the corresponding gain in BPSK was 4.7 dB. Similarly, in the coded case, OFDM begins to outperform OTFS even at relatively high coding rates such as 0.642. This behavior can be explained through the different IS structures of the two waveforms. OFDM exhibits a concentrated IS structure, whereas OTFS produces a fully spread IS structure. Under higher-order constellations such as 16-QAM, these interference characteristics become considerably more important than in the BPSK case because the Euclidean distance between constellation points is smaller. Hence, the soft symbols become more sensitive to interference, leading to lower-quality LLRs and degraded detection performance, particularly for OTFS.

E. BER Comparison Between MP and the Proposed VB-LLR

We present the BER vs. SNR under the MP and proposed VB-LLR data detector in both uncoded and coded communications ($R = 0.554$) for OTFS in Fig. 11c. We use the same simulation settings for both MP and VB-LLR: identical modulation and coding configurations, frame dimensions, equalizer initialization, and iteration counts. The results show that the BER of the VB-LLR detector matches that of MP across a broad range of SNRs while maintaining substantially lower computational complexity and simpler iterative updates, as discussed in Sec. VI-C.

VIII. Discussions and Conclusions

We developed a TF-domain analytical model for SS and IS in OFDM and OTFS, revealing their distinct characteristics–TF diversity, interference structure, and SIR–and how these vary with $\tau_{\max}$ and $\nu_{\max}$. Using this, we showed that in uncoded transmission, OFDM and OTFS perform comparably in flat-fading channels, and OTFS outperforms OFDM in all other channels due to its inherent TF diversity. In terms of performance across different equalizers, OFDM performs poorly under a 1-tap equalizer and DD-spread channels, as its performance is SIR-limited. Its performance improves dramatically under an FC-MMSE equalizer, and improves by a further 1-2 dB under a VB-LLR equalizer. OTFS, on the other hand, exhibits a diversity-SIR tradeoff and significantly outperforms OFDM under a 1-tap equalizer. Its performance improves with the FC-MMSE/VB-LLR equalizers, but to a lesser extent than OFDM. OFDM is unaffected by the delay spread $\tau_{\max}$, while OTFS improves with $\tau_{\max}$ up to a saturation point. With increasing Doppler spread $\nu_{\max}$, OFDM degrades under 1-tap but shows a slow monotonic improvement under FC-MMSE/VB-LLR. The performance of OTFS improves initially but sharply worsens under 1-tap, and improves monotonically with $\nu_{\max}$ under FC-MMSE/VB-LLR. In coded transmission, OFDM performs on par with OTFS at low code rates under 1-tap/FC-MMSE and even at moderate rates under VB-LLR, and outperforms OTFS at lower rates due to its concentrated IS structure. For both waveforms, performance improves with $\tau_{\max}$ under all equalizers, and improves over a wider range of $\nu_{\max}$ under 1-tap equalizer compared to the uncoded case, while improving monotonically with $\nu_{\max}$ under VB-LLR.

The engineering takeaways based on the simulation settings considered in this paper are as follows: i) When the channel is flat-fading, the choice between OFDM and OTFS does not matter, irrespective of the receiver structure employed. ii) When the channel is purely delay-spread, a low-complexity 1-tap equalizer is sufficient for both OFDM and OTFS. Furthermore, in coded communication systems, OFDM can achieve performance comparable to OTFS. iii) When the channel is purely Doppler-spread or DD-spread, receiver sophistication becomes important. Among the considered receivers, VB-LLR achieves the best performance, followed by FC-MMSE and then the 1-tap equalizer. Moreover, in uncoded systems and coded systems with relatively high code rates, OTFS outperforms OFDM. iv) When a sophisticated receiver (e.g., VB-LLR) is employed together with coded communication at moderate code rates, the choice between OFDM and OTFS becomes largely inconsequential. v) At sufficiently low code rates, OFDM becomes the preferred waveform. For example, in the considered settings, OFDM outperforms OTFS at code rates of approximately $R \leq 0.301$ with VB-LLR detection, and for $R \leq 0.117$ with 1-tap equalization. vi) The above observations are based on lower-order constellations such as BPSK. For higher-order constellations such as 16-QAM, OFDM remains an attractive choice even at relatively high code rates. For example, with VB-LLR detection, OFDM outperforms OTFS at a code rate of $R \leq 0.642$.

Future work may focus on theoretical analysis of how the IS structure interacts with different equalizers, extending the proposed framework into a universal analytical tool for comparing different waveforms, and investigating the performance under practical nonidealities (e.g., non-rectangular pulse shaping and imperfect CP), advanced coding techniques [31], and with multiple antennas.

References

[1] J. G. Andrews, S. Buzzi, W. Choi, S. V. Hanly, A. Lozano, A. C. K. Soong, and J. C. Zhang, "What will 5G be?" *IEEE J. Sel. Areas Commun.*, vol. 32, no. 6, pp. 1065–1082, 2014.

[2] W. Jiang, B. Han, M. A. Habibi, and H. D. Schotten, "The road towards 6G: A comprehensive survey," *IEEE Open J. Commun. Soc."*, vol. 2, pp. 334–366, 2021.

[3] C.-X. Wang, X. You, X. Gao, X. Zhu, Z. Li, C. Zhang, H. Wang, Y. Huang, Y. Chen, H. Haas, J. S. Thompson, E. G. Larsson, M. D. Renzo, W. Tong, P. Zhu, X. Shen, H. V. Poor, and L. Hanzo, "On the road to 6G: Visions, requirements, key technologies, and testbeds," *IEEE Commun. Surveys Tuts.*, vol. 25, no. 2, pp. 905–974, 2023.

[4] Y. Hong, T. Thaj, and E. Viterbo, *Delay-Doppler Communications: Principles and Applications*. Academic Press, 2022.

[5] R. Hadani, S. Rakib, M. Tsatsanis, A. Monk, A. J. Goldsmith, A. F. Molisch, and R. Calderbank, "Orthogonal time frequency space modulation," in *Proc. WCNC*, 2017, pp. 1–6.

[6] Z. Wei, W. Yuan, S. Li, J. Yuan, G. Bharatula, R. Hadani, and L. Hanzo, "Orthogonal time-frequency space modulation: A promising next-generation waveform," *IEEE Wirel. Commun.*, vol. 28, no. 4, pp. 136–144, 2021.

[7] P. Raviteja, K. T. Phan, Y. Hong, and E. Viterbo, "Interference cancellation and iterative detection for orthogonal time frequency space modulation," *IEEE Trans. Wireless Commun.*, vol. 17, no. 10, pp. 6501–6515, 2018.

[8] P. Raviteja, Y. Hong, E. Viterbo, and E. Biglieri, "Effective diversity of OTFS modulation," *IEEE Wireless Commun. Lett.*, vol. 9, no. 2, pp. 249–253, 2020.

[10] W. Anwar, A. Kumar, N. Franchi, and G. Fettweis, "Physical layer performance modeling of modern multicarrier modulation techniques," *IEEE Trans. Commun.*, vol. 70, no. 6, pp. 3725–3741, 2022.

[9] G. D. Surabhi, R. M. Augustine, and A. Chockalingam, "On the diversity of uncoded OTFS modulation in doubly-dispersive channels," *IEEE Trans. Wireless Commun.*, vol. 18, no. 6, pp. 3049–3063, 2019.

[11] S. K. Mohammed, "Derivation of OTFS modulation from first principles," *IEEE Trans. Veh. Tech.*, vol. 70, no. 8, pp. 7619–7636, 2021.

[12] Z. Wang, Z. Liu, F. Xing, R. Sun, and X. Ning, "Low complexity MMSE-SIC receiver for OTFS in high-speed mobile scenarios," *IEEE Commun. Lett.*, vol. 28, no. 3, pp. 667–671, 2024.

[13] Q. Li, J. Yuan, M. Qiu, S. Li, and Y. Xie, "Low complexity turbo SIC-MMSE detection for orthogonal time frequency space modulation," *IEEE Trans. Commun.*, vol. 72, no. 6, pp. 3169–3183, 2024.

[14] F. Huang, Q. Guo, Y. Zhang, and Y. V. Zakharov, "Message passing-based joint channel estimation and signal detection for OTFS with superimposed pilots," *IEEE Trans. Veh. Tech.*, vol. 73, no. 8, pp. 11 531–11 542, 2024.

[15] L. Xiang, Y. Liu, L.-L. Yang, and L. Hanzo, "Gaussian approximate message passing detection of orthogonal time frequency space modulation," *IEEE Trans. Veh. Tech.*, vol. 70, no. 10, pp. 10 999–11 004, 2021.

[16] N. Halder and C. R. Murthy, "Channel estimation and data detection in DS-spread channels: A unified framework, novel algorithms, and waveform comparison," *IEEE Trans. Signal Process.*, vol. 73, pp. 4108–4123, 2025.

[17] V. Yogesh, V. S. Bhat, S. R. Mattu, and A. Chockalingam, "On the bit error performance of OTFS modulation using discrete Zak transform," in *Proc. ICC*, 2023, pp. 741–746.

[18] P. Raviteja, E. Viterbo, and Y. Hong, "OTFS performance on static multipath channels," *IEEE Wireless Commun. Lett.*, vol. 8, no. 3, pp. 745–748, 2019.

[19] X. Huang, A. Farhang, and R.-R. Chen, "Channel estimation and turbo equalization for coded OTFS and OFDM: A comparison," *IEEE Commun. Lett.*, vol. 12, no. 9, pp. 1613–1617, 2023.

[20] B. V. S. Reddy, C. Velampalli, and S. S. Das, "Performance analysis of multi-user OTFS, OTSM, and single carrier in uplink," *IEEE Trans. Commun.*, vol. 72, no. 3, pp. 1428–1443, 2024.

[21] S. Li, J. Yuan, W. Yuan, Z. Wei, B. Bai, and D. W. K. Ng, "Performance analysis of coded OTFS systems over high-mobility channels," *IEEE Trans. Wireless Commun.*, vol. 20, no. 9, pp. 6033–6048, 2021.

[22] W. Anwar, A. Krause, A. Kumar, N. Franchi, and G. P. Fettweis, "Performance analysis of various waveforms and coding schemes in V2X communication scenarios," in *Proc. WCNC*, 2020, pp. 1–8.

[23] Y. Gong, Z. Li, L. Yang, L. Tian, J. Miao, D. Zhang, and Z. Xu, "LDPC-Hadamard code-assisted OTFS in high-mobility scenarios," *IEEE Open J. Veh. Technol.*, vol. 6, pp. 1849–1860, 2025.

[24] S. S. Das, V. Rangamgari, S. Tiwari, and S. C. Mondal, "Time domain channel estimation and equalization of CP-OTFS under multiple fractional Dopplers and residual synchronization errors," *IEEE Access*, vol. 9, pp. 10 561–10 576, 2021.

[25] M. F. Keskin, C. Marcus, O. Eriksson, A. Alvarado, J. Widmer, and H. Wymeersch, "Integrated sensing and communications with MIMO-OTFS: ISI/ICI exploitation and delay-doppler multiplexing," *IEEE Trans. Wireless Commun.*, vol. 23, no. 8, pp. 10 229–10 246, 2024.

[26] S. S. Thoota and C. R. Murthy, "Variational Bayes' joint channel estimation and soft symbol decoding for uplink massive MIMO systems with low resolution ADCs," *IEEE Trans. Commun.*, vol. 69, no. 5, pp. 3467–3481, 2021.

[27] R. Chong, S. Li, Z. Wei, M. Matthaiou, D. W. K. Ng, and G. Caire, "Cross-domain iterative detection for OTFS transmission with frequency domain equalization," *IEEE Trans. Commun.*, vol. 73, no. 10, pp. 9886–9902, 2025.

[28] S. Tiwari, S. S. Das, and V. Rangamgari, "Low complexity LMMSE receiver for OTFS," *IEEE Commun. Lett.*, vol. 23, no. 12, pp. 2205–2209, 2019.

[29] Z. Wei, W. Yuan, S. Li, J. Yuan, and D. W. K. Ng, "Off-grid channel estimation with sparse Bayesian learning for OTFS systems," *IEEE Trans. Wireless Commun.*, vol. 21, no. 9, pp. 7407–7426, 2022.

[30] "3GPP TS 38.214 v16.2.0 (2020-07); NR physical layer procedures for data," 2020."

[31] Z. Zhang, M. J. Ahmadi, K.-K. Wong, J. Dang, Z. Zhang, C. Masouros, and C.-B. Chae, "Joint pattern, data, and channel estimation for unsourced random access in gmac and mimo systems," *IEEE Trans. Wireless Commun.*, vol. 25, pp. 21 433–21 448, 2026.